

School of Civil Engineering
Faculty of Engineering



UNIVERSITY OF LEEDS

CIVE5455

Individual Research Project Dissertation

Submitted in partial fulfilment of the requirements for the degree of
MEng in Advanced Concrete Technology

**Does structural synthetic fibre reduce or eliminate
the well documented size effect phenomena
prevalent in concrete structures?**

by

Desmond Vlietstra

September 2018

Does structural synthetic fibre reduce or eliminate the well documented size effect phenomena prevalent in concrete structures?

Abstract

Size effect is a well-documented phenomenon that effects structures in plain and reinforced concrete. Rilem introduced a size effect factor into their design methodology for steel fibres - SFRC, (Rilem TC 162 TDF) after it was found that this design method over- estimated the results based on notched beam tests. No information is given on how this size effect criterion was derived or its background other than stating that it is not well understood and that this is an area that requires more research.

The Model Code 2010 states that any fibre can be used as long as it meets the design requirements. With the lack of codes for macro synthetic fibre reinforced concrete, the obvious starting point is to use an established steel fibre methodology such as Rilem TC 162 TDF. But the question arises as to if there is a possibility that macro synthetic fibre behaves differently to steel fibre with respect to size effect and if so to what extent. The purpose of this thesis is to understand the effect that synthetic fibre has on the well documented fracture mechanics size effect of plain and reinforced concrete and if the existing size effect criterion applied to steel fibre in this design methodology should be applied when considering synthetic fibre.

The question therefore arises. Does structural synthetic fibre reduce or eliminate the well documented size effect phenomena prevalent in plain and reinforced concrete?

This study considered geometrically similar notched beam tests of fibre reinforced prisms with the largest beams being twice the size of a standard EN14651 Beam. The major findings indicated that while the size effect is very obvious at the crack initiation. Post crack the synthetic fibre changes the brittle behaviour of the concrete which is prone to size effect introducing a more plastic behaviour thereby reversing the size effect and introducing what appears to be an increased load bearing capacity relative to size.

Acknowledgements

Concrete is a complex matrix of many individual components that together form a rock like material. A Thesis which in its whole is viewed as an individual accomplishment is no different from concrete in this respect. The “Individual accomplishment” can only be achieved by a large number of components in this case People that have come together in various ways to bond and form that rock-solid matrix. Making that accomplishment possible.

This thesis is the fruition of three years of hard work, comprising of two years of course work and a one year of research project, none of which would have been possible without the people who have been part of it in some form or other. Without the ardent support of my wife Caroline Doeglas. The constant coffee, meals, motivation when needed, acceptance and support of late nights, early mornings, and endless weekends, the counsel, and belief in me. I simply cannot thank you enough without this amazing support this would have been an unsurmountable mountain. I would also like to acknowledge my supervisor Dr Emilio Garcia-Taengua and Prof Phil Purnell, My Boss, Tony Cooper thank, you for your amazing support on both a personal and professional level and often wise counsel. Dr Ralf Winterberg, for your technical support, Peter Karoly Juhasz and Peter Schaul of JKP Static Ltd. For your assistance at the Czako Adolf Laboratory of the Department of Mechanics, Materials and Structures at Budapest University of Technology and Economics, from sourcing and manufacture of moulds, The testing and making sense of the reams of data, to the disposal of the broken beams and everything in between. Mathew Clements CEO of Elasto Plastic Concrete for the financial assistance with my studies and Yoshi Hagihara CEO of Barchip Inc for the financial support of the research testing. My colleagues at work, Susan Grantham, Jamie Higgs, Craig Wright, Todd Clarke, Paul Clayton you have all played various roles in the successful outcome of this work and finally my children Paul and Suzanne Vlietstra. And off course anyone else who I have not named, a thesis can only be written on the background and support of friends, colleagues and relatives. Thank you to everyone who made this possible.

Contents

Abstract.....	ii
Acknowledgements.....	iii
Chapter 1 Fracture Mechanics of Concrete.....	1
1.1 Introduction	1
1.2 Concrete a composite material.....	1
1.3 Linear Elastic and Nonlinear Fracture Mechanics	2
1.4 Fracture of Concrete	4
Chapter 2 Size Effect	7
Chapter 3 Fibre Reinforced Concrete	11
3.1 Fibre – Basic Concepts and Terminology	11
3.2 Types of Fibres	14
3.3 Micro or Macro Synthetic Fibres?.....	15
3.4 Fibres for structural use	16
3.5 Fibre and mix consistency.....	19
Chapter 4 Characterization and Responsiveness of FRC.....	22
4.1 Response in tension.....	22
4.1.1 Strain / Deflection: Hardening and Softening.....	23
4.2 Response in Flexure	26
4.2.1 Limit of proportionality.....	26
4.2.2 Residual flexural tensile strength.....	27
4.2.3 Fracture energy	28
4.3 Post Crack Behaviour (Toughness)	29
Chapter 5 Test methods to characterize & evaluate FRC.....	31
5.1 Uniaxial Tension Tests.....	31
5.1.1 Rilem TC 162 TDF Uni-axial tension.	31
5.1.2 JSCE Dog bone Test.....	33
5.2 Flexural beam tests.....	34
5.2.1 EN 14561 Test method - Measuring the flexural tensile strength	34
5.2.2 Rilem TC 162-TDF Bending Test.	35
5.2.3 Fib Model Code 2010	36

5.2.4	JCI-S-002-2003 Method of test for load – displacement curve.	36
5.2.5	ASTM C1609 For flexural performance of FRC	36
5.2.6	JCI–S-003-2007 Test for bending moment-curvature curve.	37
5.2.7	JSCE-SF4 Test for Flexural Strength and Flexural Toughness	37
5.2.8	EN14488-3 Flexural strengths (first peak, ultimate and residual)	38
5.3	Flexural plate tests	39
5.3.1	ASTM C1550 Round Panel Test.	39
5.3.2	EN14488-5 Square panel test.	40
5.3.3	EFNARC Three Point Bending Test on notched square panel.	41
Chapter 6	Approaches to analyse the flexural behaviour of FRC	42
6.1	Rilem Stress Strain ($\sigma - \epsilon$) approach to analyse flexural behaviour.	42
Chapter 7	Experimental Programme	45
7.1	Hypothesis	45
7.2	Background to hypothesis	45
7.3	Determination of hypothesis	47
7.4	Testing Outline	48
7.4.1	Introduction	48
7.4.2	Summary of Testing.	48
7.4.3	Determination of required test specimens	48
7.5	Test specimen details	49
7.6	Moulds	50
7.7	Macro Synthetic Fibre	52
7.8	Mix Design	53
7.8.1	Mix details	53
7.8.2	Mix proportioning	55
7.9	Test Setup	57
7.9.1	Crack width measurement	57
Chapter 8	Results and Discussion	59
8.1	Large beams	59
8.2	Medium beams	60
8.3	Small beams	62

8.4	Standard Beams	63
8.5	Comparison of beam results.	64
8.5.1	Load – CMOD.....	64
8.5.2	Residual flexural tensile strength.....	65
8.5.3	Introducing the Bazant size effect law into the data set.....	67
8.5.4	Introducing the equivalent angle method of calculating size effect.	67
8.5.5	Discussion	70
Chapter 9	Conclusions.....	73
References.....		74
Appendix 1. Raw measurements		78
Appendix 2. Summaries of results Load/Force-CMOD		86
Appendix 3. Bazant law data		88
Appendix 4. Equivalent angles and Bazant law data		90
Appendix 5. Previous Assignments		93

Chapter 1 Fracture Mechanics of Concrete

1.1 Introduction

Fracture mechanics can be broadly summed up according to Bazant (Bazant, Z.B. and Planas, 1998) as a failure theory, using energy criteria in conjunction with strength criteria, taking into account the propagation of failure through the structure.

At the time of writing his book, fracture mechanics had been widely accepted in the failure analysis of metal structures in fields such as aerospace, nuclear engineering and naval but can be described as new in the field of concrete structures. Bazant cites the reason for this as being due to the forms of fracture mechanics till “recently” as being only applicable to homogeneous brittle materials such as glass and homogeneous brittle-ductile metals. “With concrete structures one must consider strain softening due to distributed cracking, localization of cracking into larger fractures prior to failure and bridging stresses at the fracture front.

There would appear to be two distinct schools of thought with regards fracture mechanics, with a lot of building codes ignoring the theory of fracture mechanics and instilling a Factor of safety into the design. A report by the ACI Committee 446 (ACI, 1991) states that the most compelling reason to consider fracture mechanics is the size effect.

1.2 Concrete a composite material.

Concrete is defined by the American Concrete Institute (ACI, 2018b) as a mixture of hydraulic cement, aggregates, and water, with or without admixtures, fibres, or other cementitious materials. Concrete can therefore be considered a heterogeneous material. Research shows that the characteristics of the individual components very much define the overall characteristics of the composite. The macroscopic material behaviour of concrete is influenced by the geometry, spatial distribution and material properties and mutual interactions of the individual material constituents (Keerthy and Kishen, 2016). Any book on mix design such as those by Day and Lydon (Lydon, 1982) (Day et al., 2017) go to great lengths to point out amongst others, the most

common law about concrete being Abram's law which states that the strength of a concrete mix is inversely related to the mass ratio of the water to cement and therefore as the water content increases, the strength of concrete decreases. To quote Rao: "Abrams' water/cement ratio law, pronounced during 1918, has been described as the most useful and significant advancement in the history of cementitious materials technology, in general, and in the concrete technology, in particular." (Rao, 2001).

In the same vein a lot of literature such as (Siriga et al., 2017) and (Beygi, M.H.A. et al., 2013) comment on how aggregate occupies more than 70% of the volume of a concrete mix and for that reason it is pivotal in determining the mechanical and physical properties of the concrete in both the hardened and fresh state. Like so many available text books (Kosmatka and Wilson, 2016) dedicate an entire chapter to aggregates. Discussing at length the importance of grading, volume fraction, shape, surface texture and compressive strength to name but a few, of the very many attributes necessary for an aggregate to be considered, fit for purpose. Taking into consideration how these attributes will affect the overall composite mix in both its plastic and hardened state. While this is a very broad subject in its own right, this section of work will concentrate on the fracture process and explore briefly how it is affected by some of the constituents selected in the mix design process.

1.3 Linear Elastic and Nonlinear Fracture Mechanics

The Theory of fracture mechanics of concrete is a derivative of nonlinear fracture mechanics (NLFM) based on its guiding principal of crack propagation with an extensive fracture process zone (FPZ) which prevails ahead of the crack. This as explained by Shi (Shi, 2009) is largely developed from the theory of linear elastic fracture mechanics (LEFM)

Linear elastic fracture mechanics (LEFM) has been around for almost 100 years starting with what Karihaloo (Karihaloo, 1995) describes as " A Celebrated Paper by Griffith (1920)" prior to which there was no explanation to the differences between theoretically predicted and the real tensile strengths of hard brittle materials. A proposal by Griffith in 1920 of his energy approach for the brittle fracture of glass,

essentially based on the theory that all materials, including extremely smooth homogeneous materials such as glass, contains imperfections, which could be as small as microscopic flaws. These flaws could be cracks, pores and dislocations to name but a few. Flaws such as cracks introduce high stress concentrations near their tips. This theory is really on the microscale of tunnelling where an excavation is placed in rock which causes a redistribution of the surrounding stress field, dependant on shape of excavation and direction of stresses, the measured stresses on the corners of the excavation can be as high as eight times the actual stress. (Hoek and Brown, 1982). In fracture mechanics this is often referred to as the stress concentration factor K_t , not to be confused with the stress intensity factor.

In the 1960's it was realized that linear fracture mechanics could not be applied to concrete and the first significant attempt to develop a non-linear fracture mechanics framework was taken.

The imperfections based on Griffiths theory and summarised by Van Mier (van Mier, 2013) are the source of stress concentrations, which may lead to the failure of the material at a level well below its theoretical strength. In considering the crack tip stresses, and based on the Griffith fracture theory “ The energy stored in the system must be sufficient to overcome the fracture energy of the material” (Shi, 2009) Irwin generalized the concept in his theory of brittle fracture by defining an energy release rate G (In honour of Griffith) which is the measure of the available energy for a unit extension of the crack and is representative, as Irwin states, (Irwin, 1957) “ of the force tending to cause crack extension” and a stress intensity factor K . The stress intensity factor K defines the stress state at the crack tip and displacement fields, while the energy release rate G represents the driving force to open that crack (Shi, 2009)

There are three possible modes of deformation at a crack tip as illustrated in figure 1.1 The opening mode commonly known as mode 1, which is of most interest in concrete is where the load is applied normal to the crack plane and therefore tends to open the crack. , Mode 2 depicts in plane shear where the surfaces of the two cracks slide against each other and mode 3 depicts out of plane shear. This mode does not occur in the plane elastic problem.

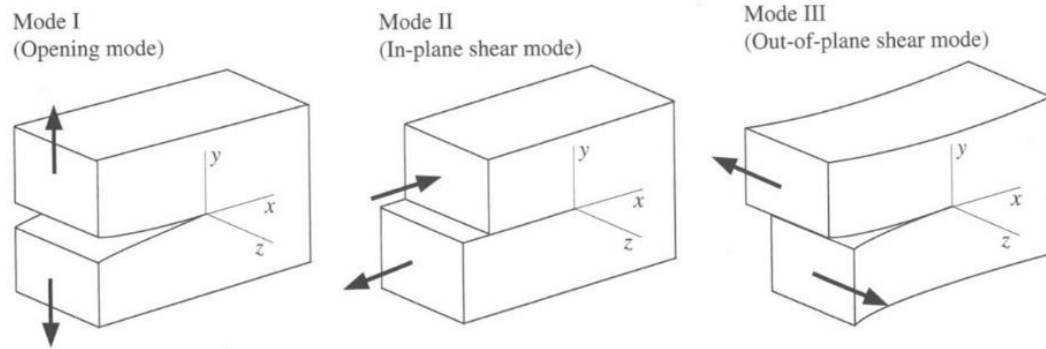


Figure 1.1 Three modes of deformation at a crack tip after Shi (Shi, 2009)

A number of authors such as Kesler and Walsh are listed by Bazant (Bazant, Z.P., 2002) as having successfully concluded that LEFM of sharp cracks was inadequate for normal concrete structures, Bazant goes on to describe that Hillerborg contributed a major advance in concrete fracture in 1976, inspired by the FPZ instituted earlier for non-concrete materials. Bazant credits Hillerborg as being pivotal in improving and adapting the cohesive crack model to concrete. Utilizing their finite element analysis showing that the cohesive crack model, which is also known as the fictitious crack model correctly predicts a deterministic size effect, for the flexural failure of unnotched plain concrete. This differs from the Weibull statistical size effect with further refinements by Peterson who strengthened this conclusion. (Bazant, Z.P., 2002)

1.4 Fracture of Concrete

While toughness is the post crack measure of the efficiency of fibre it is important to consider how the cracks develop in concrete, and in turn how the concrete matrix interacts with the fibre. This interaction is well described by Juhász (Juhász, 2013) who describes the concrete as being a bi-component material which consists of a gravel frame filled with cement grout, which when combined provides the matrix with its tensile strength, compressive strength and ductility. The fibres only start to work after a crack has been initiated and at this point provide additional ductility to the matrix. Zollo (Zollo, 1997) suggests that the crack arrest mechanism for FRC is similar to the way in which aggregate fillers absorb energy by arresting micro cracking in concrete. Due to the cumulative effect of large numbers of fibres, which individually

can be absorbing energy and controlling the crack growth by a number of mechanisms such as fibre rupture, fibre pull out, fibre bridging, and de bonding at the fibre/matrix interface. Bridging and fibre pull-out produces the highest added ductility to the concrete. Both these mechanisms, according to Juhász (Juhász, 2013), depend on the strength of the cement grout for the bonding action which is dependent on the type of cement and very importantly the water / cement ratio which has a direct relationship to the structure of porosity of the interstitial transition zone (ITZ) where it plays a critical role. (Prokorski and Langier, 2000)

There have been many studies of the effect of the water / cement ratio and its effect on the fracture parameters and brittleness of concrete. Beygi (Beygi, M.H.A. et al., 2013) completed 154 notched beam tests of varying water cement (W/C) ratios ranging between 0.7 – 0.35. These results showed that with a decrease in W/C ratio the fracture toughness increased linearly, with a smoother fracture surface. This can be attributed to the improved bond strength between the paste and the aggregates caused by an increase in fracture energy, with cracks more likely to pass across an aggregate than through the ITZ. Again, this shows that the quality of the ITZ and cement paste is dependent on the W/C ratio.

A series of three point bending tests carried out by Karamloo (Karamloo et al., 2016) showed that an increase in aggregate size increased the fracture toughness, and the fracture energy increased. While Beygi showed that there is a linear increase in the fracture toughness when the volume fraction of the coarse aggregate is increased.(Beygi, M.H. et al., 2014).

There are a number of toughening mechanisms that define the fracture process of concrete at the crack tip on the micro scale. One such mechanism that resists the crack propagation is the bridging action of the aggregate, which Simon (Simon and Kishen, 2016) defines as bridging stress. With failure in the concrete eventually occurring due to the deterioration of the bond between the binding matrix and the aggregate. Wittmann suggests that a three-level approach namely macro, meso and micro levels should be used to model the failure of concrete. Concrete is considered as a homogeneous isotropic material which makes use of effective material properties at the macro level.

At the meso level concrete is seen as three components being the aggregate, the matrix and the aggregate matrix interface. The crack propagation can be explained as being a failure of either the coarse aggregate itself or of the bond between the matrix and the aggregate as depicted in figure 1.2, and finally at the micro level, the fine aggregates as well as the cement paste and the cement paste / fine aggregate interface. At this level the disparity of the combination of different parts along with pores and other microscopic flaws complicates the failure mechanism and “limits the application of classical fracture mechanics on concrete.” (Wittman, 1983). . Figure 1.3 depicts a linear fracture in concrete showing the linear zone, the nonlinear zone and the fracture process zone at the micro level.

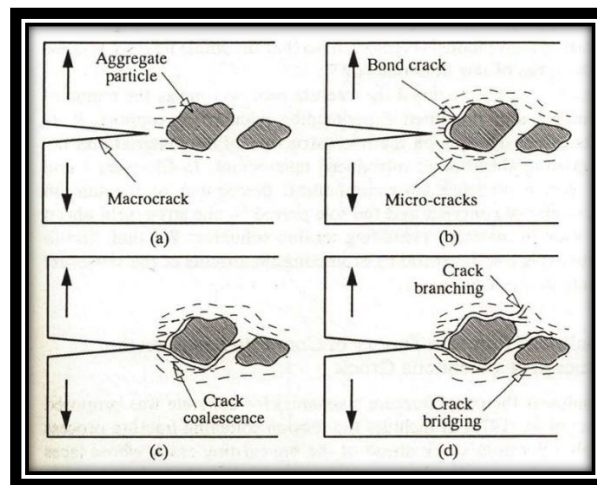


Figure 1.2 Schematic representation of the fracture process zone development
After (Karihaloo, 1995)

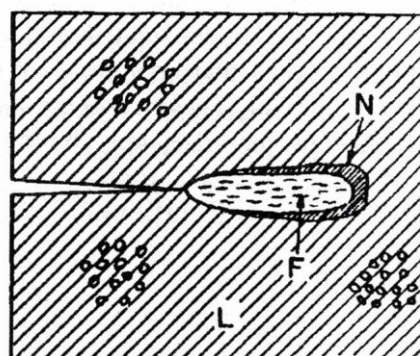


Figure 1.3 Showing the Linear Zone (L), Non-Linear Zone (N) and the Fracture Process Zone (F) in concrete. *After (ACI, 1991)*

Chapter 2 Size Effect

Size effect is described by van Mier (van Mier, 2013) as one of the salient characteristics of fracture mechanics. Size effect is by no means a new science, Both Leonardo da Vinci and Galileo studied size effect on strength, figure 2.1 shows a quote and illustration taken from a translated manuscript originally written by Galileo in 1638.

“Among heavy prisms and cylinders of similar figure, there is one and only one which under the stress of its own weight lies just on the limit between breaking and not breaking: so that every larger one is unable to carry the load of its own weight and breaks; while every smaller one is able to withstand some additional force tending to break it.”

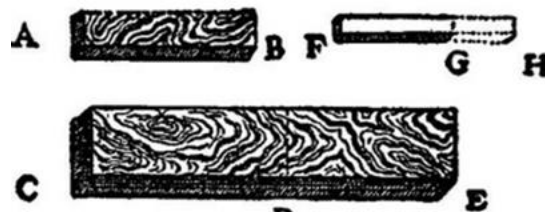


Figure 2.1 Quote and illustration from Galileo illustrating his thinking along the lines of scaling and size effect. (Galileo, 1638)

The question around size effect that does arise is to what degree the strength of real-size buildings and structures can be predicted from small scale laboratory tests. Van Mier goes on to explicate the size effect is a consequence of fracture mechanics, where the version of fracture mechanics predicts that larger structures fail at relatively smaller loadings. Based on them being generally weaker and their behaviour weaker.(van Mier, 2013)

The size effect of concrete is discussed by Ozbolt as being a well-known phenomenon with two aspects being statistical and deterministic. Ozbolt has considered both experimental and theoretical studies in his paper, referencing papers as far back as 1962, and quotes Bazant as stating that the main reason for the size effect “lies in the release of strain energy due to fracture growth” (Ozbolt et al., 1994).

The size effect, according to Bazant, is “the main consequence of fracture mechanics” and he states that “It must be taken into account in design” and that the material fracture parameters can be determined “merely from maximum load measurements, which are easy to carry out” (Bazant, Z.P. and Kazemi, 1990).

Bazant argues that while size effect is clearly evident in concrete, it is largely ignored in its own merits by design codes and the reason for minimal catastrophic failure of structures due to size effect has been limited due to the excessively high safety factors used in the design. To quote Bazant “The dead load factor in the current codes is excessive and its excessive value produces a hidden size effect for the design of large structures” (Bazant, Z.P., 2002). In summary designers are using an excessive dead load factor as a hidden substitute for the size effect.

One of Jamet’s conclusions on their paper (Jamet et al., 1995) is that there was a significant effect of the size of the specimen on its behaviour which they feel should be considered in the toughness characterization.

In solid materials a deformation can only be sustained if the load applied to the bounding surface causes a redistribution of stresses internally. The defining characteristic of an elastic material being its ability to return to its original shape once this load is removed. While most materials used in engineering possess some level of elasticity, once the load exceeds that limit of elasticity this is referred to as plastic failure. In which case the material will either fail by fracture or flow. A solid material that fails by fracture is considered to be brittle while a material that fails by flow is considered plastic. The load at which the material is no longer able to return to its original shape is considered the elastic limit or yield strength of that material, beyond the yield strength permanent deformation will occur. The proportionality limit is that point up to which the stress is proportional to the strain as defined by Hooke’s law. When plotted on a stress strain curve the stress strain graph is a straight line, and the gradient will be equal to the elastic modulus of the material.

The strength of geometrically similar structures according to the classical theories on plasticity or limit analyses are independent of structure size as the critical stress is not dependent on the structure size. However concrete structures and any other structure

manufactured from brittle or quasibrittle materials, by their nature do not follow this trend and show strong size effect as their cracking stress is dependent on the specimen or structure size.

With the size effect being understood according to Bazant, as the dependence of the structure strength on the structure size. The strength can be conventionally defined as the nominal stress at peak load which is defined as proportional to the load divided by a typical cross-sectional area. Bazant has derived the following equation; (Bazant, Z.B. and Planas, 1998)

$$\sigma_N = c_N \frac{P}{bD} \quad \text{for 2D similarity,} \quad \sigma_N = c_N \frac{P}{bD^2} \quad \text{for 3D similarity} \quad (1.1)$$

Where P = applied load, b = thickness of a 2-dimensional structure, D = characteristic dimension of the structure or specimen as depicted in figure 2.2 below. Finally c_N = a coefficient introduced for convenience. Normally $c_N = 1$, but can be changed to coincide with changes discussed later.

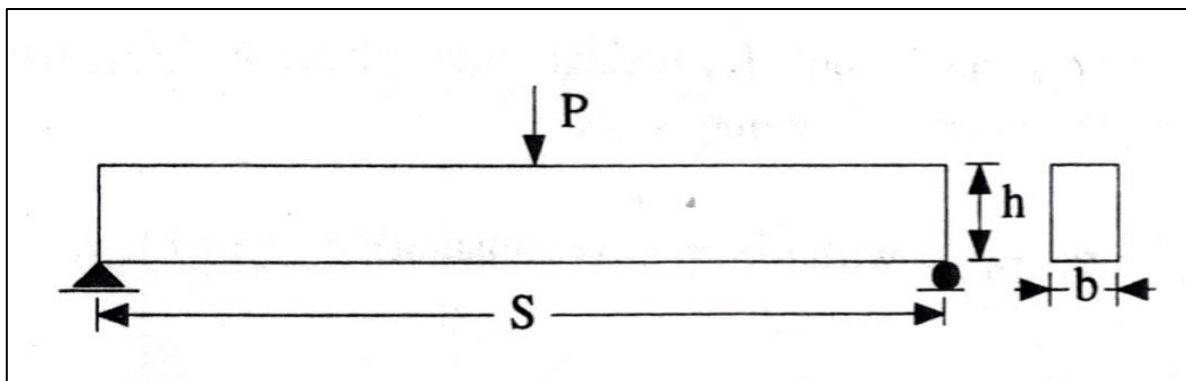


Figure 2.2 – Showing a three- point beam test with notations used in the size effect formula although in the diagram D has been substituted with h. After (Bazant, Z.B. and Planas, 1998)

Should you wish to let σ_N coincide with the plastic bending formulae for the maximum then.

$$\sigma_N = \frac{PS}{bh^2} = c_N \frac{P}{bD} \quad \text{with} \quad c_N = \frac{S}{h} \quad (= \text{constant}) \quad (1.2)$$

Alternatively, the characteristic dimension of the beam span instead of the beam depth ($D=S$) in which case the formula is rewritten as:

$$\sigma_N = \frac{3PS}{2bh^2} = c_N \frac{P}{bD} \quad \text{with} \quad c_N = 1.5 \frac{S^2}{h^2} \quad (= \text{constant}) \quad (1.3)$$

We may choose σ_N to coincide with the formula for the maximum shear stress near the support according to the elastic bending theory in which case we have $D=h$.

$$\sigma_N = \frac{3P}{4bh} = c_N \frac{P}{bD} \quad \text{with} \quad c_N = 0.75 \quad (= \text{constant}) \quad (1.4)$$

Finally using the span as the characteristic dimension ($D=S$) we may write

$$\sigma_N = \frac{3P}{4bh} = c_N \frac{P}{bD} \quad \text{with} \quad c_N = \frac{3S}{4h} \quad (= \text{constant}) \quad (1.5)$$

Bazant states all these formula are valid definitions of the nominal strength for three point bent beams, although the first formula (1.1) is the most generally used. (Bazant, Z.B. and Planas, 1998).

Chapter 3 Fibre Reinforced Concrete

Concrete is an extremely versatile material mainly due to its ability to be moulded into almost any shape and geometry making it the most commonly used building material. Structures made of concrete are for a variety of reasons, prone to cracking. While mechanical loading is the most important reason, other physical loadings such as temperature gradients, differential drying and chemical attack also need to be considered as a cause of cracking and deterioration. The major cause of cracking in concrete can be attributed to the low tensile strength of concrete which seldom exceeds 10% of the concrete's compressive strength.(van Mier, 2013)

With its high compressive but low tensile strength concrete does tend to be brittle. This tensile weakness can be overcome by using conventional bar reinforcement, an alternative to which to a certain extent, is fibre of which Soutsos correctly states that “the full potential of fibre reinforced concrete is still not fully exploited in practice.”(Soutsos, 2012) The use of modern day fibre in concrete is a relatively new material however the concept dates far back in history to about 3500 years ago where ancient cultures used straw to reinforce clay bricks and even in nature where birds such as the South American Ovenbirds have used clay reinforced with grass and natural fibres to build their nests ever since time began.(Mobley, 2009).

Fibre reinforced concrete (FRC) is considered a composite material, defined by the American Concrete Institute as “a concrete containing dispersed, randomly oriented fibres.” With fibres in turn being defined as “a slender and elongated solid material, generally with a length at least 100 times its diameter.”(ACI, 2018b). The introduction of fibres into concrete gives it an “enhanced post cracking residual strength due to the capacity of the fibres to bridge the crack faces”(di Prisco et al., 2013)

3.1 Fibre – Basic Concepts and Terminology

Aspect Ratio

The fibre aspect ratio is a measure of the slenderness of individual fibres. Calculated as the length of the fibre divided by the equivalent fibre diameter.

Balling

Formation of a clump of entangled fibres forming a “ball”, this could be as a result of the properties of the fibre, or the mixing protocol or both.

Decitex

This term evolved from the textiles industry and is defined as the weight of the fibre in grams per 10 000 metres of a continuous filament of fibre. The higher the decitex the thicker the fibre.

Denier

This term while used interchangeably with decitex is defined as the weight of fibre in grams per 9000 metres of a continuous filament of fibre.

Ductility

Ductility is a measure of a material's ability to undergo significant plastic deformation before rupture. Fibre adds post cracking ductility to both concrete and shotcrete.

Embossing

Embossing is the raised or recessed pattern placed on the surface of some fibres which assists with mechanical anchorage in the concrete matrix.

Equivalent residual flexural strength

This is the average flexural stress that is measured at a specified deflection or crack width in a beam test.

Fibre reinforced concrete or fibre reinforced cement

In a large amount of literature according to (Purnell, 2010) references are made to both fibre-reinforced concrete and fibre-reinforced cement. Fibre reinforced cement refers to thin sheet material with high fibre content, which is not considered in this thesis. Fibre reinforced concrete which refers to more traditional concrete to which fibres are added, Fibre reinforced concrete more specifically reinforced with macro synthetic fibres are considered in this work.

Fibre content and volume fraction of fibres

Fibres are purchased by weight but due to the variety of densities that fibre materials are available in, the amount of fibre added to a concrete mix is often expressed as a volume fraction or a percentage of the total volume of the composite (concrete and fibres), termed "volume fraction" (V_f). V_f typically ranges from 0.1 to 3% as explained by (Naanman, 2003). Due to density differences of the various materials that fibres are manufactured from, fibres occupying the same volume of the matrix would be different weights and the mechanical properties of composites are based on the on the volume fraction and not the weight fraction of the fibres.

In normal weight concrete 1% volume of steel fibres is equivalent to approximately 80Kg/m^3 while the same volume fraction of polypropylene fibres would be about 9.1 Kg/m^3 .

Fibre Dosage

Total fibre mass or weight in a unit volume of concrete expressed either as kg/m^3 or in non-metric countries as lb/yd^3 A typical dosage of macro synthetic fibre, depending on the application would rarely be less than $2\text{-}3\text{ kg/ m}^3$ and seldom exceed 10 kg/m^3 .

Fibre count

Fibres used in concrete are often described in literature as being short, discrete, uniformly distributed and randomly orientated. A non-scientific method for quantifying the amount of fibres post-test that intersect the fracture face is the "fibre count" this is a common request when ASTM C1550 Round determinate panel testing is carried out, while it is not a prerequisite of the test. Essentially the fibres are counted on an area of $100\text{mm} \times 80\text{ mm}$ on both opposing fracture faces and merely gives an indication of fibre distribution. Care needs to be taken with counting ruptured fibres twice as Bernard, the inventor of the RDP test, states "Although fibre count on each crack face is assessed manually it is known to be corrupted by the incidence of fibre rupture."(Bernard et al., 2010).

Fibrillated fibres

This is a synthetic fibre that is designed to “split” at the ends into many thinner sections or branches to enhance the mechanical bond, this action can be pre-formed or occur during mixing.

Monofilament fibres

This is a single fibre; its cross section is usually circular or prismatic although other cross-sectional shapes are available.

3.2 Types of Fibres

Fibres come in many different materials, both natural and manufactured Purnell (Purnell, 2018) states that for fibre reinforced concrete (FRC), being a brittle matrix the requirement of the fibres is that they have a greater than >1% elongation to failure in order to counteract this brittleness. He lists the fibres described below as being used in fibre reinforced concrete, while table 3.1 shows the typical properties of a range of selected fibres.

Glass fibres – While there are four main types, AR or Z-glass is specifically for use in fibre reinforced concrete due to the zirconia content which provides high resistance to alkaline environments.

Carbon fibres – Pitch-based fibres being cheaper than PAN-based fibres are used for FRC.

Polymer fibres – which includes amongst others polypropylene, polyolefin, aramid, nylon and polyethylene and polyvinyl alcohol (PVA). These come in a variety of cross sections with differing surface treatments which could be chemical, mechanical or both to enhance bonding.

Natural Fibres – generally being of vegetable origin such as jute, flax, sisal, cotton and coir (coconut husk).

Steel fibres – these come in a variety of cross sections and shapes to enhance bonding to the concrete matrix, they can be mild steel, stainless, galvanised and even high carbon.

Fiber type	Relative density (specific gravity)	Diameter, μm (0.001 in.)	Tensile strength, MPa (ksi)	Modulus elasticity, MPa (ksi)	Strain at failure, %
Steel	7.80	100 – 1000 (4 – 40)	500 – 2600 (70 – 380)	210,000 (30,000)	0.50 – 3.5
Glass					
E	2.54	8 – 15 (0.3 – 0.6)	2000 – 4000 (290 – 580)	72,000 (10,400)	3.0 – 4.8
AR	2.70	12 – 20 (0.5 – 0.8)	1500 – 3700 (220 – 540)	80,000 (11,600)	2.5 – 3.6
Synthetic					
Acrylic	1.18	5 – 17 (0.2 – 0.7)	200 – 1000 (30 – 145)	17,000 – 19,000 (2500 – 2800)	28 – 50
Aramid	1.44	10 – 12 (0.4 – 0.47)	2000 – 3100 (300 – 450)	62,000 – 120,000 (9000 – 17,000)	2 – 3.5
Carbon	1.90	8 – 9 (0.3 – 0.35)	1800 – 2600 (260 – 380)	230,000 – 380,000 (33,400 – 55,100)	0.5 – 1.5
Nylon	1.14	23 (0.9)	1000 (140)	5200 (750)	20
Polyester	1.38	10 – 80 (0.4 – 3.0)	280 – 1200 (40 – 170)	10,000 – 18,000 (1500 – 2500)	10 – 50
Polyethylene	0.96	25 – 1000 (1 – 40)	80 – 600 (11 – 85)	500 (725)	12 – 100
Polypropylene	0.90	20 – 200 (0.8 – 8)	450 – 700 (65 – 100)	3500 – 5200 (500 – 750)	6 – 1.5
Natural					
Wood cellulose	1.50	25 – 125 (1 – 5)	350 – 2000 (51 – 290)	10,000 – 40,000 (1500 – 5800)	
Sisal			280 – 600 (40 – 85)	13,000 – 25,000 (1900 – 3800)	
Coconut	1.12 – 1.15	100 – 400 (4 – 16)	120 – 200 (17 – 29)	19,000 – 25,000 (2800 – 3800)	10 – 25
Bamboo	1.50	50 – 400 (2 – 16)	350 – 500 (51 – 73)	33,000 – 40,000 (4800 – 5800)	
Jute	1.02 – 1.04	100 – 200 (4 – 8)	250 – 350 (36 – 51)	25,000 – 32,000 (3800 – 4600)	1.5 – 1.9
Elephant grass			180 (26)	4900 (710)	3.6

Table 3.1 Properties of selected fibres (Kosmatka and Wilson, 2016)

3.3 Micro or Macro Synthetic Fibres?

With macro synthetic fibre being a more recent addition, a lot of older literature describes synthetic fibre purely as “non-structural” simply because this literature is only considering micro synthetic fibre which has been around much longer than macro synthetic fibre. Distinction therefore needs to be made here. The British standards

divides synthetic fibre into two main classes according to their physical form. Figure 3.1 clearly illustrates what micro fibres of various length look like,

Class Ia: Micro fibres: < 0,30 mm in diameter; Mono-filamented

Class Ib Micro fibres: < 0,30 mm in diameter; Fibrillated

Class II: Macro fibres: > 0,30 mm in diameter

A note made by the European standards referring to macro fibres is that Class II fibres are generally used where an increase in residual flexural strength is required.(BSI, 2006d).



Figure 3.1 showing micro synthetic fibres of various lengths

3.4 Fibres for structural use

Only steel and synthetic fibres are currently considered in European standards for structural use. Part 1 of EN 14889 specifies requirements for steel fibres, while Part 2 of EN 14889 specifies requirements for polymer fibres, both for structural or non-structural use in concrete, mortar and grout. With a common note between them giving the following definition: “Structural use of fibres is where the addition of fibres is designed to contribute to the load bearing capacity of a concrete element”.

This standard covers fibres intended for use in all types of concrete and mortar, including sprayed concrete, flooring, precast, in-situ and repair concretes. (BSI, 2006c)

Macro Synthetic fibre has been commercially available since 2000, (The-Concrete-Society, 2007) In the 18 years since their introduction there have been large improvements made in the technology with regards to improved tensile strength, increased modulus of elasticity, higher toughness with lower dose rates and engineered bonding mechanisms ensuring that the bond and snapping strength is ideally a function of the fibre length. Figure 3.2 and 3.3 respectively show a cross section of some of the steel and synthetic fibres available on the market, essentially highlighting the vast differences with regards to shape and geometry within the two categories.

In the *fib* Model Code for concrete structures 2010 fibre, reinforced concrete is recognised as a new material for structures. di Prisco sums this up as an introduction which will favour forthcoming structural applications, due to the need for adopting new design concepts and that is has been the lack of international building codes to date that have significantly limited the use of fibre reinforced concrete. di Prisco also states that considerable effort was devoted to introducing a material classification to standardize performance-based production and stimulate an open market for every kind of fibre based on performance. (di Prisco et al., 2013)



. Figure 3.2 showing a selection of steel fibre highlighting the differences in shape and size



Figure 3.3 showing a selection of macro synthetic fibre highlighting the differences between fibres

3.5 Fibre and mix consistency.

Quality concrete has very well-defined principle requirements in both the fresh and hardened state. Some of these properties such as Consistence, Workability and Cohesiveness are discussed below with a brief definitions and explanations as given in The Fundamentals of Concrete. (Owens, 2013). Following this will be a discussion on fibre in the concrete mix.

Consistence – The consistence (also called consistency in some publications) of a mix is a measure of its stiffness / sloppiness or the fluidity of the mix. The consistence of each batch should be the same for effective handling, placing and compacting. Consistence is measured using the slump test.

Workability – The workability of a mix is the relative ease with which the concrete can be placed, compacted and finished without segregation of the individual materials. It is important to note that workability and consistence are two totally different properties. Unfortunately, there is no way of measuring workability or putting a value to it, but the slump test together with an assessment of properties like the stone content, cohesiveness, and plasticity can give a useful indication.

Workability at a given consistence is influenced by the stone size, the smaller the stone size the better the workability but the higher the cost in terms of material cost. The stone content is at its optimum when there is sufficient paste to coat all the stone particles and slightly overfill the spaces between. When the stone content is too high, the resultant is the stones are too close, with minimal lubrication of paste and therefore increased friction the mix becomes too harsh making it difficult to compact and finish. If the stone content is too low the mix simply becomes uneconomical due to the high cement content.

Cohesiveness sometimes labelled stability is the resistance to segregation. The cohesiveness is dependent on the fines content, (material that passes the 0.30 mm sieve) if there is an abundance of fines the mix will be very sticky and if the fines content is insufficient then the mix will lack cohesiveness. Cement is similar in that a cement rich mix may become sticky and difficult to handle. Very often similar

statements such as this one “While macro plastic fibres effectively control plastic shrinkage cracking they do reduce workability of fresh concrete” (Yin et al., 2015) will be found in publications, All too often this statement is based on a misunderstanding of what the slump cone is really measuring, resulting in an ill formed conclusion, believing that the workability has been reduced as a result of the additional surface area of the fibre in the mix.

The surface area of sand or gravel is dependent on its shape and size and can be reported in terms of m²/g. Assuming the sand or gravel is spherical then using the formula below the surface area can be calculated.

$$a = 4\pi r^2$$

$$m = \rho V = \rho \left[\frac{4\pi r^3}{3} \right] \quad (1.6)$$

Where

a = surface area

r = radius

ρ = density

As a generalisation to simplify the explanation a single sized gravel with an effective diameter of 2x10⁻¹ will return a specific surface area of 11.1m²/g.

A single sized sand with an effective diameter of 5 x 10⁻³ will return a specific surface area of 444.4m²/g.

One kilogram of synthetic fibre, depending on type, will return an approximate surface area of between 10 and 20m²/g, so by adding 6kg of synthetic fibre to a cubic metre of concrete in terms of surface area, the additional paste demand is highly negligible and comparable to a few additional kilograms of sand and gravel in a cubic metre of concrete.

The fact that fibres are elongated compared to the aggregate means that they promote interlocking. Generally, the slump flow is decreased with increased fibre addition and the lower the initial slump the more the effect fibre has on slump reduction. However, while the fibre reduces the flow when “static” as seen in the slump test, fibre reinforced concrete tends to respond well to vibration. A properly designed FRC mix can be

placed and pumped with standard placement practices. According to the ACI the energy required to consolidate and place fresh FRC is no greater than for fresh plain concrete, It is suggested however that at moderate to high dosages of fibre the use of additional chemical superplasticisers could be used to maintain the desired slump where required. With regards to pumping, with reasonable dose rates there is seldom need for any adjusting of the mix.(ACI, 2018a)

Chapter 4 Characterization and Responsiveness of FRC.

4.1 Response in tension

The tensile strength of concrete is about eight to ten times lower than its compressive strength, and with tensile cracks present in almost every reinforced concrete structure. Van Mier suggests that Mode 1 fracture of concrete is therefore considered the most important for the fictitious crack model where the most important input parameters are the stress-strain curve and the softening diagram. (van Mier, 2013) Mode 1 fracture being an opening mode where a tensile stress acts normal to the plane of the crack, as discussed in chapter 1.3.

The direct tensile test is the most reliable method available to determine the residual properties of fibre reinforced concrete but with the complexity of the test, rarity of testing machines, the expense of each individual test and high rate of failed tests alternative indirect tensile methods are proposed.(van Mier, 2013; Amin, Ali et al., 2015; Conforti et al., 2017)

The Model Code 2010 proposed bending tests aimed at determining the load-deflection relation and using these results to derive the stress-crack width relations by inverse analyses and performing equilibrium calculations for the numerous crack openings. The beam used in the bending test is the EN 14651. The diagram illustrated in figure 4.1 is of the applied load (F) versus the deformation expressed as crack mouth opening displacement ($CMOD$). The Parameters f_{Rj} representing the residual flexural tensile strength are evaluated from the F - $CMOD$ relationship as follows:

$$f_{Rj} = \frac{3F_j l}{2bh_{sp}^2} \quad (1.7)$$

Where:

f_{Rj} is the residual flexural strength corresponding to $CMOD = CMOD_j$; [MPa]

F_j is the load corresponding to $CMOD = CMOD_j$; [N]

l is the span length; [mm]

b is the specimen width [mm]

h_{sp} is the distance between the notch tip and the top of the specimen (125mm) (Fib, 2012)

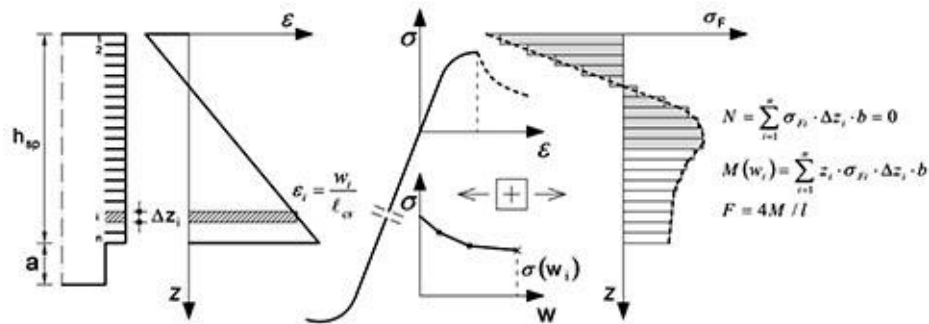


Figure 4.1 showing the inverse analysis of a beam in bending performed to obtain the stress-crack opening relation. After (Fib, 2012)

Conforti has proposed indirect tensile tests for fibre reinforced concrete. Typical proposed tests include the double edge wedge splitting test and the Barcelona test based on the fact that while the EN14651 is the reference test the Model Code MC2010 suggests, the Model Code states that with the aim of harmonizing the structural design of FRC structures it accepts other standard tests if they are proven to produce reliable correlation factors with the parameters of EN 14651. (Section 5.6.2.2 of MC2010) (Conforti et al., 2017)

4.1.1 Strain / Deflection: Hardening and Softening.

Fibre reinforced concrete exhibits a far superior ductility when compared to unreinforced concrete. Unreinforced concrete fails in tension and bending very soon if not immediately after the formation of a single crack. This is where fibre reinforced concrete differs in that its most distinctive feature is its ability to reinforce the cracked matrix. This is done by transferring through the fibres that bridge the crack, the tensile stresses that are caused by the bending which in effect hold the cracked surfaces together. Amin concurs that the degree as to how much force is carried across the crack is very dependent on the type and quantity of fibres bridging the crack. (Amin, A. et al., 2017).

Plain concrete has only the aggregate interlock which produces very limited stress transfer across the crack. The bridging activity according to Babafemi (Babafemi and Boshoff, 2017) is only triggered after a cementitious material deforms and a crack is triggered. The increase in the energy absorption and ductility is dependant on the interaction between the fibre and the matrix, the matrix in fibre reinforced concrete (FRC) being described as the interfacial transition zone (ITZ). Babafemi discusses many factors that influence the bond between the matrix and the fibre at the ITZ such as fibre type, fibre geometry, fibre surface deformation, fibre strength, fibre diameter, fibre length, elastic modulus, as well as those properties related to the concrete matrix.

A combination of these factors listed above influences the overall deformation behaviour of the composite material under load. Failure will be dictated by either the fibre pull-out or fibre rupture. This mechanism is shown in figure 4.2 below. The fibre volume fraction according to Fantilli (Fantilli et al., 2016) will cause the fibre reinforced concrete to behave differently.

If the maximum load carrying capacity of the fibre after the first crack corresponds to the first crack strength, the composite is considered to be softening, however if a higher load carrying capacity occurs subsequent to the first crack strength, then the fibre bridging strength governs and the composite is considered to be hardening.

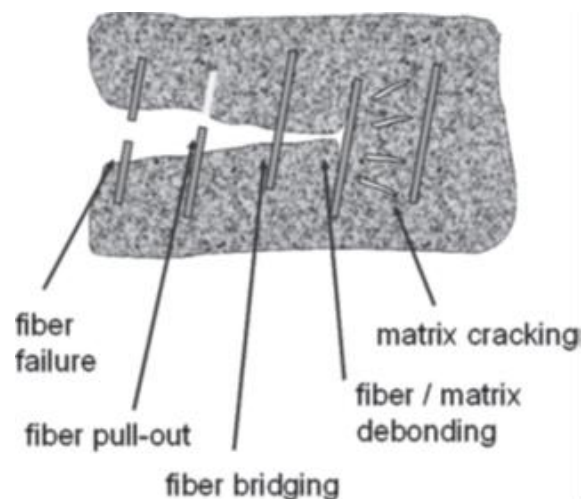


Figure 4.2 Schematic showing the mechanism in which fibre reinforcement works After (ACI, 2018a)

The stress strain curve illustrating the four possible states of concrete, being brittle (no reinforcement), strain softening, strain hardening and elastic-plastic is illustrated in figure 4.3 The stress strain curve should not be confused with the load deformation curve as shown in figure 4.4. It should be noted that the deflection hardening post cracking response is typically accompanied by multiple cracking while the deflection softening response is typically accompanied by a single crack. While this behaviour is typical, the use of notched beams could possibly reduce the formation of multiple cracking in the deflection hardening situations by the nature of the testing setup and the defined weakness caused by the single notch. There is however the alternative argument that by introducing a notch the crack is forced to occur there rather than finding the path of least resistance as it does in a unnotched beam and therefore the notch could induce a higher response.

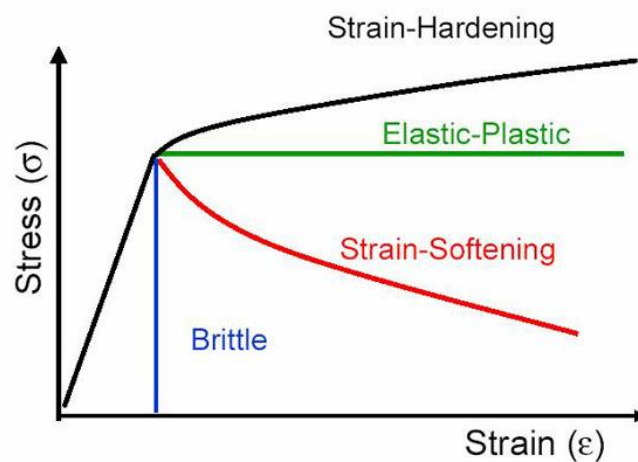


Figure 4.3 Stress – Strain behaviour of concrete (Weiss, 2011)

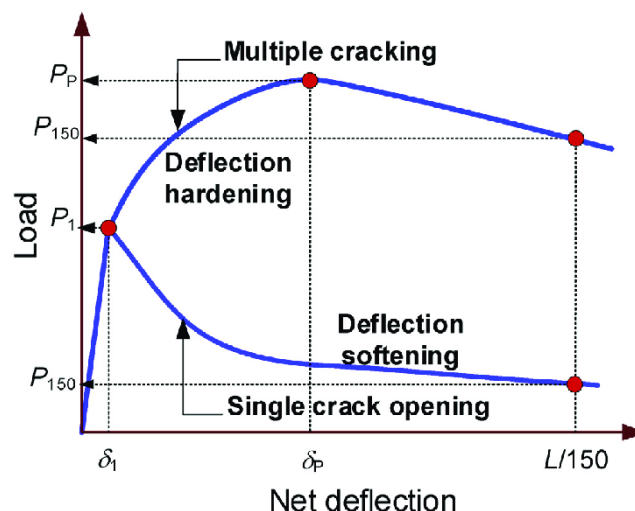


Figure 4.4 Load deflection curves showing deflection softening and deflection hardening after (Jamsawang et al., 2018)

4.2 Response in Flexure

Flexure is the action of bending and the characteristics of fibre in flexure is resolved with any number of bending tests usually in the form of a prism or plate. Both prisms and plates can be notched or unnotched depending on the test method requirements.

4.2.1 Limit of proportionality

When a load is applied to a concrete beam in the three-point bending test, the concrete initially shows elastic behaviour which according to Hooke's law generally states that the deformation is proportional to the stress applied to it. This is identified in a load deformation graph where the load – deformation is linear. With the increase in applied stress, there will be a point where the concrete will change its behaviour and the deformation will no longer be proportional to the applied stress. This point or limit is known as the limit of proportionality or LOP.

The expression to calculate the limit of proportionality and explanation as given in the European standards (BSI, 2008) is:

$$f \frac{f}{cl} L = \frac{3F_l l}{2bh_{sp}^2} \quad (1.8)$$

Where

$f \frac{f}{cl} L$ is the LOP, in Newton per square millimetre;

F_l is the load corresponding to the LOP, in Newton;

l is the span length in millimetres;

b is the width of the specimen in millimetres;

h_{sp} is the distance between the tip of the notch and the top of the specimen, in millimetres;

The load value F_l shall be determined by drawing a line at a distance of 0.05mm and parallel to the load axis of the load-*CMOD* or load deflection diagram and taking as F_l

the highest load value in the interval of 0.05mm. Therefore F_l can be described as the peak load at which point an initial crack is formed and the line deflects to shows either deflection softening or hardening.

4.2.2 Residual flexural tensile strength

In a notched beam test, where the beam is centrally loaded and once the limit of proportionality discussed previously is reached, a crack will initiate at the notch and with added deflection the crack will increase in length. The residual flexural tensile stress is a measure of the fictitious stress at the tip of the notch, which is assumed to act in an uncracked mid-span section. The centre-point load denoted as F_j and the residual flexural tensile strength is the load corresponding to a specific crack mouth opening displacement (CMOD). In the EN14651 beam test the load F_j is measured at CMOD₁ (0.5mm), CMOD₂ (1.5mm), CMOD₃ (2.5mm) and CMOD₄ (3.5mm). The expression given by EN14651 for the residual flexural strength $f_{R,j}$ is given below:

$$f_{R,j} = \frac{3F_j l}{2bh_{sp}^2} \quad (\text{N/mm}^2) \quad (1.9)$$

Where

b = width of the specimen

h_{sp} = distance between tip of the notch and top of cross section (mm)

L = span of the specimen (mm)

$f_{R,i}$ = is the residual flexural strength corresponding to CMOD_i with [i= 1,2,3,4] as shown in figure 4.5 Below

F_j = is the load corresponding to CMOD_i. (BSI, 2008)

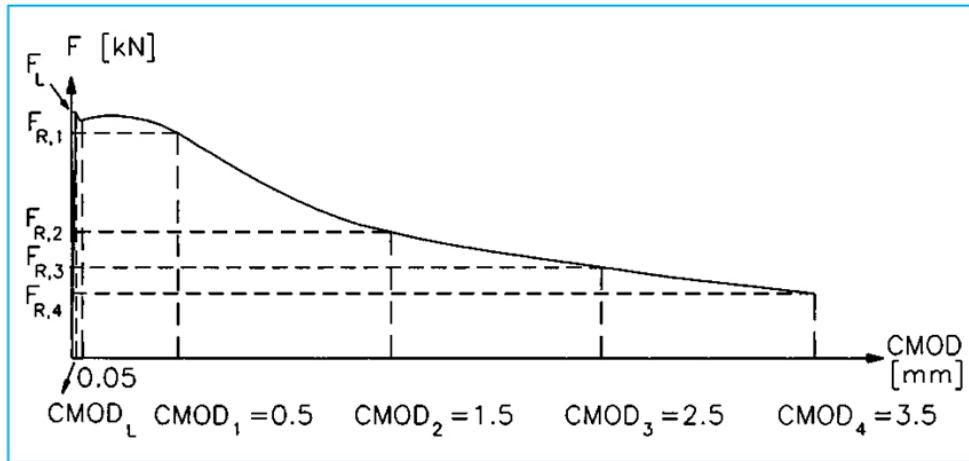


Figure 4.5 showing the residual flexural tensile strength and corresponding CMOD's (RILEM_TC_162-TDF, 2003)

4.2.3 Fracture energy

The fracture energy can be calculated to three significant figures and is described as part of the Japanese Concrete Institute test JCI-S-001-2003. Collection of the data follows the procedure of the Japanese Concrete Institute three-point notched beam test JCI-002-2003 which is briefly described in section 4.5.2 under flexural tests. The formula and explanation to calculate fracture energy is as follows:

$$W_1 = 0.75 \left(\frac{S}{L} m_1 + 2m_2 \right) g \cdot CMOD_c \quad (1.10)$$

Where:

G_F = fracture energy (N/mm²)

W_0 = area below CMOD curve up to rupture of specimen (N.mm) (4 significant figures)

W_1 = work done by deadweight of specimen and loading jig (N.mm)

A_{lig} = area of broken ligament (b x h) (mm²)

M_1 = mass of specimen (kg)

S = Loading span (mm)

L = total length of specimen (mm)

M_2 = mass of jig independent of testing machine but placed on specimen. (kg)

g = gravitational acceleration (9.807 m/s²)

$CMOD_c$ = crack mouth opening displacement at the time of the rupture (mm)

(JCI, 2003)

4.3 Post Crack Behaviour (Toughness)

Toughness in the context of fibre reinforced concrete refers to the post crack behaviour. Which according to Jamet (Jamet et al., 1995) is a measure of the energy absorption capacity of the composite which is obtained experimentally. The primary reason for adding fibres to concrete is to improve the energy absorbing capacity of the composite. The performance can be measured in a bending test and evaluated by determining the area under the stress strain or load deflection curve. (Balaguru and Shah, 1992). Figure 4.6 shows an example of a stress strain graph and the different curves from plain and fibre reinforced concrete, the toughness will be the area under the curve. The performance however is influenced by a number of factors such as the beam geometry, specifically its depth, the aggregate, surface area or dimensions of the fibre, test method and fibre orientation (Conforti et al., 2017) added to this list is fibre type, fibre geometry, fibre volume fraction and loading rates (Balaguru and Shah, 1992)

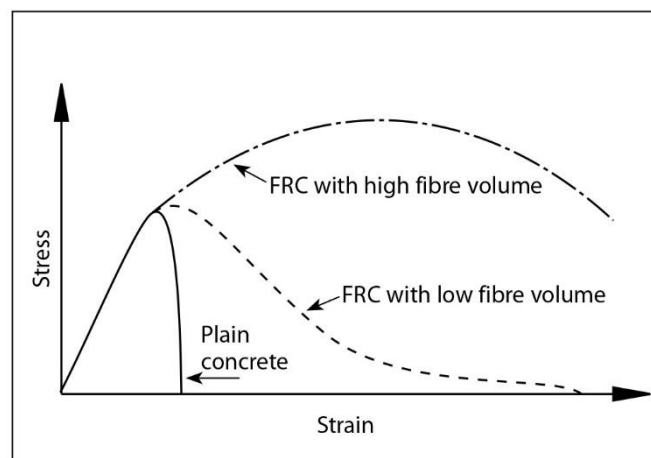


Figure 4.6 Example of the behaviour of plain and FRC .(The_Concrete_Institute, 2013)

Research according to (Yin et al., 2015) has found that macro synthetic fibre has no obvious effects on the flexural strength of the concrete, and that the main benefit is the improved ductility in the post crack region and the greatly improved flexural toughness of the concrete. The conclusion from their testing indicated that macro synthetic fibres had no impact on the compressive strength of the matrix either. The main benefits being the improved ductility in the post crack region, high energy

absorption capacity, improved flexural toughness and good crack controlling capacity on the drying shrinkage and providing long term residual strength due to the composite action. The residual strength and toughness being a consequence of the bridging action of the fibre across the crack. (Bakhshi et al., 2014).

The fibre type and volume fraction will impact the toughness, with a higher volume fraction of fibre providing more energy absorbing capacity or toughness due to providing more resistance in the tension zone, the critical volume will depend on the fibre characteristics with regards mix ability. (Balaguru and Shah, 1992) It goes without stating that the quality of the fibre in terms of bond, fibre length, pull out resistance and tensile strength all plays an extremely important role in achieving the toughness and different fibres will achieve same toughness with different volume fractions.

Chapter 5 Test methods to characterize & evaluate FRC.

It is necessary in structural engineering to quickly and reliably verify the material properties proposed for a structure with ease and ensure compliance between the design and the in-situ materials. Toughness characterization is essential as it can be used for relating the fundamental material behaviour to structural performance. (Jamet et al., 1995).

Paegle (Paegle et al., 2015) cites the Fib Model code 2010 (Fib, 2012) as emphasizing the significance of defining suitable material parameters which are not limited to post-peak tensile behaviour for structural design. Stating that any structural element made with randomly distributed fibres should be dimensioned with the load carrying capacity verified, regardless of if it has traditional reinforcement or not. Furthermore the post cracking strengths of the material should be determined. In order to obtain the description and mechanical characterization of fibre reinforced concrete there are a number of available test methods which can derive the post-cracking response of fibre reinforced concrete and these can be divided into three main categories

- Uniaxial tension tests with either a prescribed single crack or possible multi cracking.
- Flexural beam tests which under either three or four-point loading and performed on either notched or un-notched prisms.
- Flexural plate tests

The more common tests with basic descriptions are listed below. A large number of the tests listed below have variations.

5.1 Uniaxial Tension Tests

5.1.1 Rilem TC 162 TDF Uni-axial tension.

This requires a cylindrical specimen with a nominal diameter and length of 150 mm. The cylinder is notched circumferentially to a depth of 15mm +/- 1mm the notch width

should be between 2-5mm. Maximum aggregate size is 32mm and maximum fibre length of 60mm.

The specimen is glued to metal plates, rigidly connected to the machine. The gluing procedure is shown in figure 5.1 and the test setup is shown in figure 5.2. The specimen is tested in direct tension at a displacement rate of 5µm/min up to a displacement of 0.1mm and 100µm/min until completion of the test (at a displacement of 2mm). The expected results from this test is a stress deformation curve and a stress crack opening curve. (RILEM_TC_162-TDF, 2001)

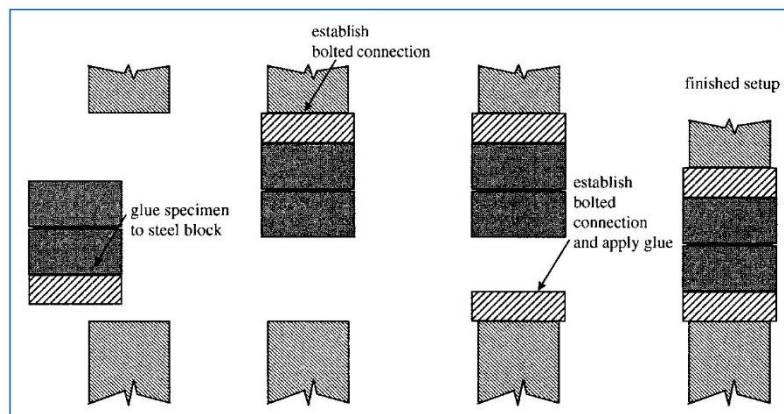


Figure 5.1 Schematic representation of the testing procedure when using adhesives to attach the specimen to metal plates in the testing machine. After (RILEM_TC_162-TDF, 2001)

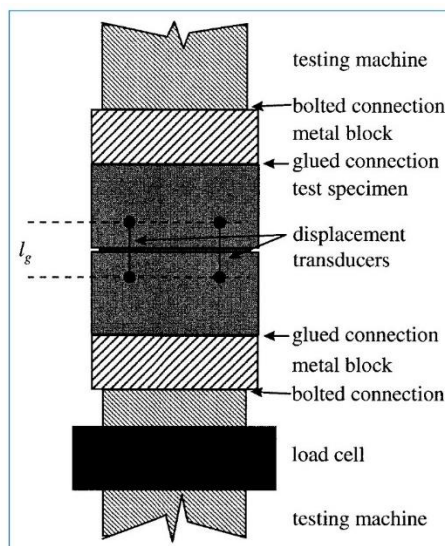


Figure 5.2 showing the test setup used for the uniaxial tension test. after (RILEM_TC_162-TDF, 2001)

5.1.2 JSCE Dog bone Test.

This is a tensile stress - strain test where a dogbone specimen with a length of 330mm and thickness of 13 or 30mm and representative cross section of $l=80\text{mm}$, $w = 30\text{mm}$ $t = 13$ or 30mm . The minimum specimen thickness (t) is based on $t \geq \text{fibre length}$ and $t \geq 2 \times \text{maximum aggregate size}$. The setup and result output is shown in figure 5.3.

This test is intended for FRC with a hardening post cracking response and requires vertical alignment between the chucks, has fixed support on one end and pin support on the other, with a constant deformation rate of 0.5mm/min . LVDTs should have a precision of $1/1000^{\text{th}}$ mm or higher.

Expected results from this test are a stress strain curve, tensile yield strength, maximum stress in the strain hardening region and, tensile strength and ultimate tensile strain. (JSCE., 2008)

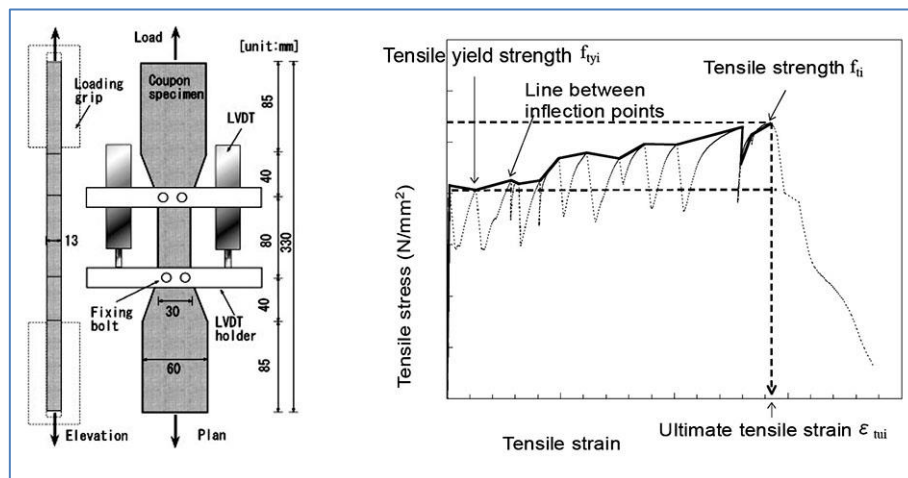


Figure 5.3 Schematic showing the unconfined tensile test using a dogbone specimen and the output showing the tensile yield strength and tensile yield strain. After (JSCE., 2008)

5.2 Flexural beam tests

5.2.1 EN 14561 Test method - Measuring the flexural tensile strength

This is a three-point bending test using a notched beam where both the width and depth = 150mm and the span (measured between the supports) = 500mm but the actual length of the beam is $\geq 550\text{mm}$ and $\leq 700\text{mm}$. The notch is cut on the side 90 degrees from cast orientation to a depth of 25mm \pm 1mm. The beam setup with dimensions is shown in figure 5.4 The beam is tested after 28 days and the maximum size aggregate should not exceed 32mm and maximum length fibre should not exceed 60mm. An image of the test in progress is shown in figure 5.5 with a closeup image in figure 5.6 showing the detail of the CMOD measuring clip which is placed between 2 knife edges, the knife edges are glued in place.

Expected results are a Load – CMOD curve, Limit of proportionality (LOP) and a residual flexural strength. (BSI, 2008)

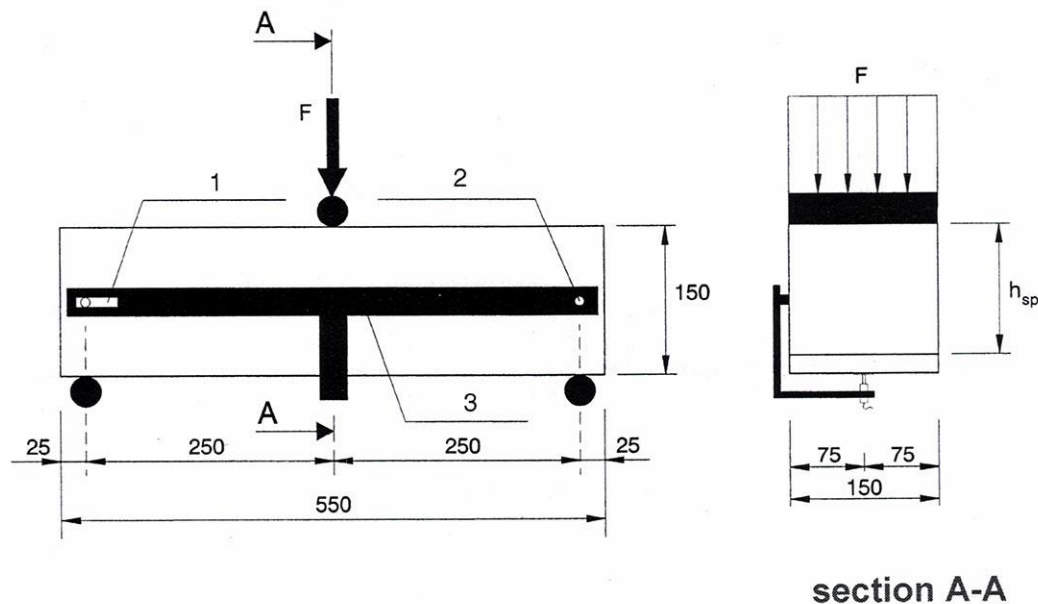


Figure 5.4 showing a schematic of the EN14651 Three-point beam test after (BSI, 2008)



Figure 5.5 showing an image of the EN14651 Three-point beam test.



Figure 5.6 Showing a close up of the CMOD clip gauge below the notch.

5.2.2 Rilem TC 162-TDF Bending Test.

This test is identical to the EN14561 test with additional expected results of energy absorption capacity (Area under the curve) Equivalent flexural strengths and residual flexural strengths at CMOD 0.5mm, 1.5mm, 2.5mm and 3.5mm. (RILEM_TC_162-TDF, 2002)

5.2.3 Fib Model Code 2010

This test is identical to EN14561 and Rilem TC 162 TDF with additional expected results of classification from ratio of characteristic residual strengths at serviceability / ultimate limit states.

5.2.4 JCI-S-002-2003 Method of test for load – displacement curve.

This is a three-point bending test of a notched beam with the following geometry where specimens shall be beams of rectangular cross section with a notch at the mid-length to a depth of 0.3 times the beam depth. The depth of the cross section (D) of the specimen shall be not less than 4 times the maximum aggregate size (d_a) The width of the cross section (B) of the specimen shall be not less than 4 times the maximum aggregate size (d_a). The loading span (S) shall be 3D. The total length of the specimen (L) shall be not less than 3.5D. The notch depth (a_0) and notch width (n_0) shall be 0.3D and not more than 5mm, respectively.

The expected results are the Load – CMOD curve and the poly linear inverse analyses cohesive stress – crack opening. (JCI-S-002, 2003)

5.2.5 ASTM C1609 For flexural performance of FRC

This is a four-point bending test of a beam without a notch. The dimensions of the beam are the following: Span $\geq 3 \times$ Diameter + 50mm ≥ 350 mm, Span $\leq 2 \times$ Diameter + Length, Width $\geq 3 \times$ fibre length, width = diameter = 150mm if length of fibre is 50 – 75mm The aggregate must be in accordance with ASTM C31 or ASTM C42 if fibre is $\leq 1/3$ diameter. An image of the beam setup is shown in figure 5.7. The frame around the beam is independent of the testing machine and is to hold the LVDT measuring displacement in place.

Expected results are first peak and peak load, strength and corresponding deflections, residual load and strengths at deflections of L/600 and L/150. Toughness and equivalent flexural strength ratio at a deflection of L/150. An image of the ASTM1609 beam test in figure 5.7 below shows the test setup and crack which in this instance is slightly off centre. (ASTM_C_1609, 2012)

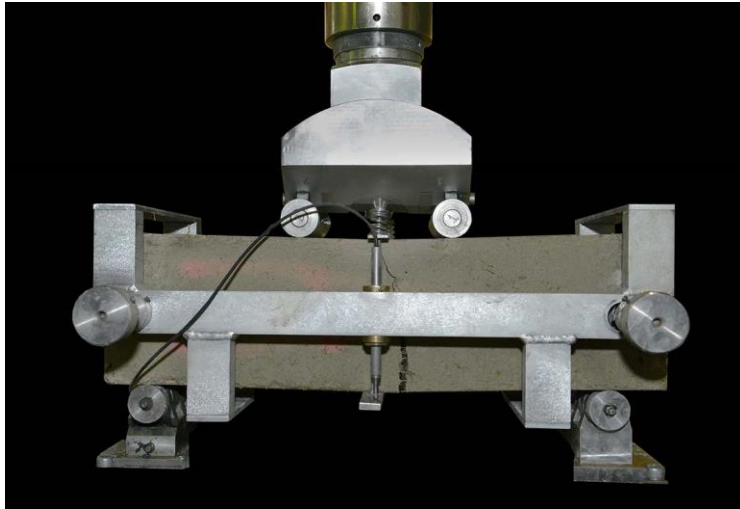


Figure 5.7 Showing the ASTM1609 beam test

5.2.6 JCI-S-003-2007 Test for bending moment-curvature curve.

This is a four-point beam test without a notch, the dimensions of the beam are width and diameter of 100mm and a total length of 400mm. The span length is 300mm, the beam is made in accordance with JIS A 1106. And the fibre should be ≤ 40 mm. Curvature is measured using 2 LVDTs in positions of 15mm and 85mm from the lower surface of the test specimen.

The expected results are stress strain and moment curvature. tensile strength and ultimate tensile and compressive strain.

5.2.7 JSCE-SF4 Test for Flexural Strength and Flexural Toughness

This is a four-point beam test without a notch. The specimen size is not specified except that the span must be three times the specimen height. The width and height of the failed cross section has to be measured at three locations to the nearest 0.2mm these measurements are then averaged and reported to four significant digits. To determine the bending toughness exactly, deflections must be measured at the locations of loading points, however it is permissible normally to only measure at the middle of the span. Figure 5.8 shows this test in progress where only the central deflection is being measured (middle of the span) by means of a linear variable differential transformer (LVDT).

The expected results from the test should give the flexural strength, residual flexural strength, flexural toughness and equivalent flexural strength. These results should be the average of a minimum of four tests.(JSCE., 2008)



Figure 5.8 showing the JSCE-SF4 four-point beam test in progress with only the central deflection being measured.

5.2.8 EN14488-3 Flexural strengths (first peak, ultimate and residual)

Essentially for shotcrete, this is a four-point beam test where the specimen shall be a sawn prism with the dimensions of 75mm depth, 125mm width and at least 500mm length. The prisms shall be cut from a sprayed panel. The loading of the prism shall be at 0.25mm / min until a deflection of 0.5mm is reached after which the speed can be increased to 1.0mm / min. the test will continue until the mid-span deflection exceeds 4mm or the specimen fractures.

The expected results from this test is the first peak, ultimate flexural strengths and residual flexural strengths. The ultimate flexural strength f_{ult} will be calculated from the maximum load recorded P_{ult} . On completion of the test the width and depth of the fracture plane must be measured with two measurements and averaged. If the fracture plane is outside the rollers then the results should be discarded.

Each flexural strength should be calculated as an equivalent elastic tensile strength. (BSI, 2006a)

5.3 Flexural plate tests

5.3.1 ASTM C1550 Round Panel Test.

This is a simply supported centrally loaded round panel test for testing fibre reinforced concrete or fibre reinforced shotcrete (sprayed concrete) often referred to as the round panel test. Its dimensions are an 800mm diameter \pm 10mm and a thickness of 75mm $-5/+15$ mm. The panels can be either cast or sprayed into a mould. After demoulding the panel is tested at the required days by placing in a testing machine where it is supported on three symmetrically arranged pivots. The load is applied through a hemispherical-ended steel piston that is advanced at a displacement of 4.0 ± 1.0 mm/min up to a central displacement of at least 45mm.

The panel experiences biaxial bending which relates to the mode of failure related to the in-situ behaviour of sprayed concrete structures. The expected results from this test is a peak load and a load deflection curve.

the toughness is ordinarily defined at central deflections of 5, 10, 20 or 40mm and if the load and net deflections are recorded in units of newtons (N) and millimetres (mm) or kilonewtons (Kn) and metres (m) then the resulting measure of energy will be in units of Joules (J)

The standard does provide correction factors for peak load and energy absorption based on the measured geometry of the panel tested.(ASTM, 2010)



Figure 5.9 Showing the ASTM C1550 RDP test setup.



Figure 5.10 Showing a closeup of a round panel on completion of the test.

5.3.2 EN14488-5 Square panel test.

This test requires fibre reinforced concrete (sprayed concrete) to be sprayed into a mould which measures 600mm x 600mm. Immediately after spraying the concrete must be trimmed to a thickness of 100mm and the slab must be cured in the mould according to EN 12390.2 for a minimum of three days. The slab is supported on a 20mm thick rigid square steel frame with a 500 mm internal dimension (the outside 50mm diameter of the slab will sit on this frame) The loading block centrally placed will also be square with a 100mm x 100mm dimension and 20mm thickness.

A suitably stiff bedding material such as mortar or plaster should be placed between the slab and the support frame as well as between the loading block and the slab. The displacement shall be at 1mm/min until the central deflection exceeds 30mm.

The expected results from this test is a load deflection curve and an energy absorption capacity reported as the area under the load deflection curve between 0 and 25mm. (BSI, 2006b)

5.3.3 EFNARC Three Point Bending Test on notched square panel.

The dimensions of the specimen are 600mm x 600mm with a nominal thickness of 100mm. The test specimens are generally sprayed and cured according to EN 12390-2 for a minimum of 3 days. A notch at mid span on the base of the panel with a maximum width of 5mm and a depth of 90mm must be wet sawn. Testing is usually carried out at 28 days.

The specimen is placed on steel rollers that have a 30mm diameter and are 600mm in length and spaced 500mm apart. A third roller of the same dimension is used to centrally load the specimen. All rollers need full contact with the specimen. If the testing machine can control the rate of increase of the CMOD then it should be operated so that the CMOD increases at a constant rate of 0.05mm/min. Once the CMOD reaches 0.2mm the rate can be increased to a speed where the CMOD increases at a rate of 0.2mm/min. The test can be terminated once the CMOD value exceeds 5mm. If the crack starts outside of the notch then the test shall be rejected.

The expected results from this test is an equivalence between CMOD and deflection, Limit of proportionality, residual flexural strength, and a load – CMOD diagram. The standard gives a table whereby the deflections and CMOD can be matched and evaluated against the EN 14651 Beam test. (EFNARC, 2011)

Chapter 6 Approaches to analyse the flexural behaviour of FRC

Quantifying the residual tensile strength or load carrying capacity of fibre reinforced concrete in a cracked section according to Gribniak. (Gribniak et al., 2012) is one of the most critical points in fibre reinforced concrete theory. There have been two approaches developed by RILEM TC 162 TDF to analyse the flexural behaviour of Fibre reinforced concrete. Both methods describe the same materials. With the stress strain approach being more widely used and pertinent to this work it will be discussed below.

6.1 Rilem Stress Strain ($\sigma - \epsilon$) approach to analyse flexural behaviour.

The Rilem TC162 Stress – Strain approach relates the stress to the fictitious strain in a certain region around the crack in which the problem required to be solved as described by Erdem (Erdem, 2003), is to be able to determine the length of the zone where the beams curvature is larger than what it would be based on the theory of elasticity, in order to calculate the strain. He further describes the σ - ϵ model as having been put forward with the intention of establishing an effective, yet simple, design tool for practicing engineers.

The main difference in the approach used for fibre reinforced concrete compared to normal reinforced concrete is that FRC has a post cracking resistance enabling the concrete to carry a tensile load across the crack. (Martinez, 2006) The compressive strength of concrete as well as the fibre fraction and geometry of fibre influences the residual flexural strengths (Lee, 2017).

The σ - ϵ design method proposed by Rilem TC 162-TDF is based on Eurocode 2. The design parameters in the stress strain relationship are determined using prismatic notched beams, This test method has since been adopted by BS EN 14561:2005 Test

Method for Metallic fibre concrete – Measuring the flexural tensile strength (Limit of proportionality (LOP), residual) (BSI, 2008)

There are a number of properties of the concrete as well as some constants that need to be known to define the criterion of the Rilem σ - ϵ model discussed below.

Compressive strength (f_{ck})

The design principles are based on the characteristic 28 day strength, which is defined as RILEM states “ that value of strength below which no more than 5% of the population of all possible strength determinations of the volume of concrete, are expected to fall” (RILEM_TC_162-TDF, 2003) using either the cylinder strength f_{ck} or the cube strength $f_{ck.cube}$.

Flexural tensile strength

The estimated mean and characteristic flexural tensile strength of fibre reinforced concrete can be derived from the following equations using the determined compressive strength f_{ck}

$$f_{fctm.ax} = 0.3(f_{fck})^{\frac{2}{3}} \quad (\text{N/mm})^2 \quad (2.1)$$

$$f_{fctk.ax} = 0.7 f_{fctm.ax} \quad (\text{N/mm})^2 \quad (2.2)$$

$$f_{fc.ax} = 0.6 f_{fct.fl} \quad (\text{N/mm})^2 \quad (2.3)$$

$$f_{fctk.fl} = 0.7 f_{fctm.fl} \quad (\text{N/mm})^2 \quad (2.4)$$

Residual flexural tensile strength.

Rilem TC 162-TDF 2003 refers to a crack mouth opening displacement (CMOD) for determining the residual flexural tensile strength using equation (2.1) where the residual flexural tensile strength f_{R1} and f_{R4} are determined following $CMOD_1$ and $CMOD_4$ respectively. These values are determined using a three point bending test. (RILEM_TC_162-TDF, 2003)

$$f_{R.i} = \frac{3F_{R.i} L}{2bh_{sp}^2} \text{ (N/mm}^2\text{)} \quad (2.1)$$

As discussed in section 4.3.2.

Chapter 7 Experimental Programme

7.1 Hypothesis

Does structural synthetic fibre reduce or eliminate the well documented size effect phenomena prevalent in plain concrete?

7.2 Background to hypothesis

Fibre for structural reinforcement of modern day concrete has been available for 50 years with macro synthetic fibre becoming available in the last 20 years according to the concrete society. (The-Concrete-Society, 2007). Although it has only been in more recent times that the full extent of its usefulness has begun to be understood and realized; Introducing fibres to concrete gives the “concrete a significant tensile residual strength in the cracked phase and reduces crack propagation”.(Buratti et al., 2010) Giaccio correctly states that when it comes to designing concrete structures using fibre “it has been widely recognised that a criterion based only on strength is not enough for FRC characterization and that it is necessary to consider the post-peak behaviour and the gains in toughness.” (Giaccio et al., 2008).Despite 50 years of steel fibre and 20 years of macro synthetic fibre availability there is currently a very limited number of recommendations or guidelines for using fibre, with most existing methods predominantly aimed at steel fibre although it is generally accepted as stated in the model code 2010 that where macro synthetic fibre meets the required performance they can be used in place of steel fibre. According to M. di Prisco “The implementation of fibre reinforced concrete (FRC) in the *fib* Model Code 2010 is a very important milestone. In the near future it will probably lead to the development of structural rules for FRC elements in Eurocodes and national codes.” (di Prisco et al., 2013). Macro Synthetic fibre is slowly starting to become more accepted by a select few in the design community and is currently used as a sole reinforcement in applications such shotcrete linings, slab on grade, certain pre-cast elements, and more recently in precast segmental tunnel linings. Macro Synthetic fibre is also used in a multitude of applications to compliment and at times reduce the existing conventional reinforcement.

The biggest barrier to more extensive use of macro synthetic fibre is as pointed out above, the lack of generally accepted design methods due to the need for refinement of the existing guidelines and recommendations with the inclusion of a design method for macro synthetic fibre reinforced concrete (MSFRC) in the current national codes. One of the most common design methods currently used was produced by Rilem known as Rilem TC 162-TDF Test and design methods for steel fibre reinforced concrete $\sigma - \epsilon$ design method. Final recommendation. (RILEM_TC_162-TDF, 2003). This design method makes use of a three point notched beam test which Rilem TC 162-TDF documented as a “Bending Test” (RILEM_TC_162-TDF, 2002) this three point notched beam test has since been standardised as the EN14651 test method for metallic fibre. (BSI, 2008) The design method has been adopted as the method of choice for the fib Model Code 2010 as well.

The Rilem TC 162-TDF discusses how their design method for steel fibre was originally developed without size-dependant safety factors and that when the results of various sized elements were compared to the predicted results based on their design method a severe overestimation was revealed. To correct this overestimation, they introduced a size dependant safety factor as shown in figure 7.1, which also shows the Rilem stress strain diagram.

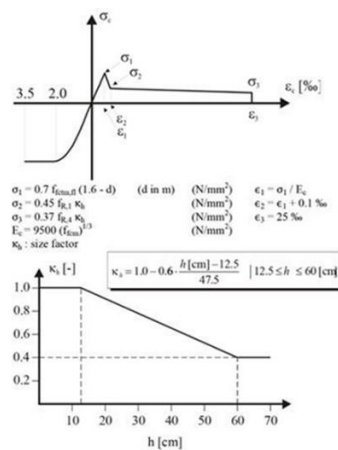


Figure 7.1 Stress Strain diagram and size factor K_h (RILEM_TC_162-TDF, 2003)

Rilem then makes the following statement with regards the size effect. “It should be outlined that the origin of this apparent size-effect is not yet fully understood. Further investigation is required in order to identify if it is due to a discrepancy of material

properties between different batches, to a size-effect intrinsic to the method or a combination of both.”(RILEM_TC_162-TDF, 2003)

Due to the limited design options available the synthetic fibre industry has by default, adopted the Rilem design method including the use of the Rilem size effect safety factor for designs using macro synthetic fibre. The question does arise as to if this size effect safety factor is applicable to macro synthetic fibre as well and if so to what extent.

7.3 Determination of hypothesis

Despite an extensive search of the available literature there seems to be a lack of research into determining the size-effect of macro synthetic fibre reinforced concrete across a series of notched beams with varying depths. And the majority of published work considers only plain concrete and a limited amount considering steel fibre and often the default experiments are based on either using standard beams as the large beams and a series of geometrically similar beams of smaller sizes or pure finite element analyses. The size dependant safety factor that has been found in the literature survey to date is described above and aimed specifically at steel fibre reinforced concrete design.

For this reason, my hypothesis takes the form of a question.

Does structural synthetic fibre reduce or eliminate the well documented size effect phenomena prevalent in concrete structures?

The aim of my research was aimed to identify if the size effect should be a consideration when designing with macro synthetic fibre and if so to what extent. Although finding a fully conclusive answer could entail further research.

7.4 Testing Outline

7.4.1 Introduction

There have been a number of highly scientific experiments carried out to consider size effect mostly of plain concrete. One of the recent experiments being carried out by Hoover and Bazant (Hoover et al., 2013) describes a test comprising a total of 164 concrete specimens of which 128 were fracture specimens cast in precision crafted moulds with 36 companion cylinders. An interesting deviation from many previously recorded classical size effect tests on plain concrete was that while the beams were geometrically similar in terms of depth and span they all maintained a common width of 40mm. The beams were cured under environmentally controlled conditions for 13 months before being tested with highly sophisticated, state of the art equipment and automated measuring devices. While this is a best-case scenario the testing reflected below was carried out under extremely tight time constraints with an even tighter budget and minimal availability of automated instrumentation, with all crack propagation measurements being manually read using hand held precision instruments. All of which will be described below.

7.4.2 Summary of Testing.

Testing based on EN14651 of a range of geometrically similar notched beams of different sizes, cast from a 50 MPa concrete reinforced with only Macro Synthetic Fibre with a view to discovering if there is a size effect on synthetic fibre reinforced concrete, and if so to what extent does fibre improve the outcome. Other outcomes hoped for is a better understanding of the crack propagation of synthetic fibre reinforced concrete.

7.4.3 Determination of required test specimens

The EN 14651 Test method for metallic fibre was developed based on the Rilem TC 162-TDF Bending test. Requiring a prism of 150mm x 150 mm cross section and a total width of 550mm to enable a span of 500mm to be tested. A saw cut notch of

25mm depth is placed at the mid-section, giving an effective depth of 125mm see figures 5.4 – 5.6 In section 5 for images of the EN14651 test being performed, as well as a description of the test method.

EN14651 beams were therefore the obvious choice as control specimens, due to the coefficient of variation realized from testing such beams a decision was made to test 7 beams reinforced with macro synthetic fibre and three beams with no reinforcing. To reduce the coefficient of variation on the actual size effect part of the experiment the decision was made to maintain the test set of beams at a constant 300mm width.

The size effect set of beams would have three depths with the small beams having a depth of 150mm (same as a standard beam), the large beams would be double that at 300mm and the intermediate beams would be half way, with a depth of 225mm. Initially it was felt that the notches should remain the same depth throughout the beams to reduce variability across the experiment, but on considering the span to depth geometries of the beams, and to ensure this was constant, the notches had to be varied proportionally according to the depth and span of the beam. The final geometries are tabulated in table 6.1 A more in-depth explanation of the testing rationale will follow in a separate paragraph.

7.5 Test specimen details

A total of twenty-two beams were cast along with companion cubes for compressive strength testing and a cylinder to determine the young's modulus of the concrete.

The beam configurations are shown in table 7.1 below with those being designated as ST being standard EN14651 beams, while the designation S, M, and L stands for small, medium and large,

Designation	Actual Dimensions					Effective Dimensions				Reinforcing
	Number of Beams	Width	Length	Depth	Notch	Effective Depth	Effective Span	Effective Span:Depth	Effective Face area	
ST - FRC	7	150	550	150	25	125	500	4	18750	Synthetic Fibre
ST - Plain	3	150	550	150	25	125	500	4	18750	Plain
S - FRC	3	300	550	150	25	125	500	4	37500	Synthetic Fibre
S - Plain	1	300	550	150	25	125	500	4	37500	Plain
M - FRC	3	300	750	225	37.5	187.5	700	4	56250	Synthetic Fibre
M - Plain	1	300	750	225	37.5	187.5	700	4	56250	Plain
L - FRC	3	300	1050	300	50	250	1000	4	75000	Synthetic Fibre
L - Plain	1	300	1050	300	50	250	1000	4	75000	Plain

Table 7.1 Beam configuration of beams used for experiment

The concrete was batched by hand using the laboratory mixer. Due to the total required amount of concrete and available facilities it was not possible to cast these specimens from the same batch of concrete however extra attention was paid to the mixes to ensure they were as similar as possible. After batching and casting, the moulds were placed on a vibrating table to ensure uniform compaction. The batching, moulding and curing were all carried out in the laboratory in the same environmental conditions, however again due to the size and weight of the large specimens and available facilities it was not possible to consider wet curing these. Therefore, a decision was made to air cure all the samples to maintain conformity as much as possible across all the samples.

7.6 Moulds

The standard beams were cast in standard machined steel moulds, while the non-standard beams required custom made “one use only moulds”. Due to the size and weight, a special base was also designed and manufactured for the moulds so they could be lifted and placed on the vibrating table for consolidation after casting. Figure 7.2 shows one of the actual moulds used for the large beams and figure 7.3 shows the conceptual design of the large mould together with the lifting base. Lifting hooks were also cast into the non-standard beams to assist with lifting at various stages such as demoulding, notch cutting and placement in the testing machine. Figure 7.4 shows the size configuration of all the cast beams. The smallest beam being a standard 150 x 150 x 600 EN14651 beam, and the largest being 300 x 300 x 1050mm.



Figure 7.2 showing the mould used for a large beam.

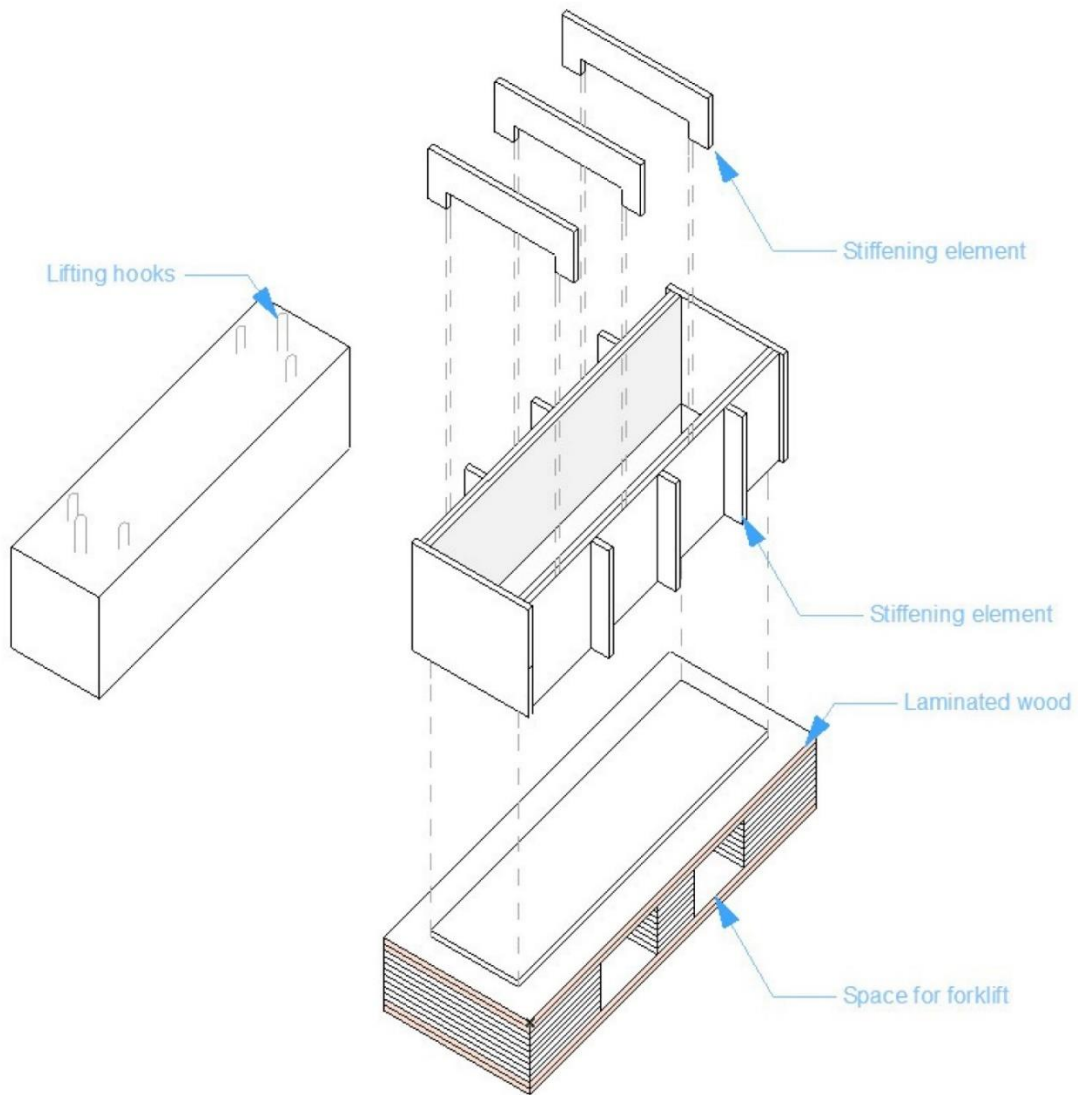


Figure 7.3 conceptual design of moulds for large beam specimen.

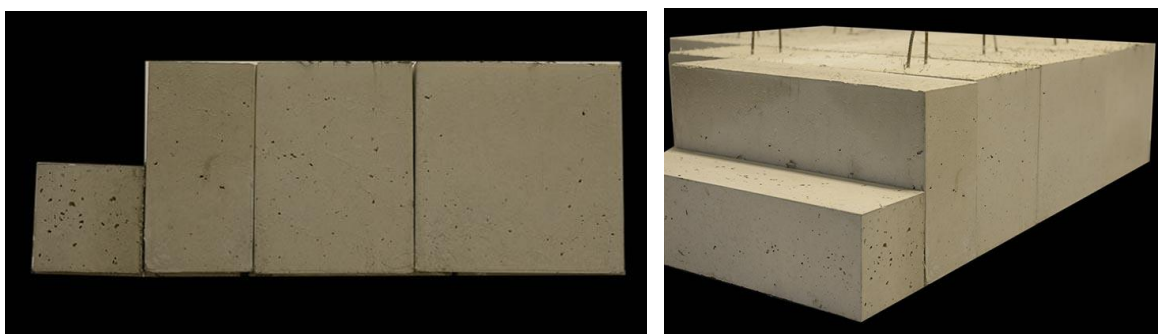


Figure 7.3 Showing the different sized beams alongside each other after casting the smallest being a standard EN14651 Beam.

7.7 Macro Synthetic Fibre

The structural macro synthetic fibre used in the experiment was BarChip48, which is a high-performance structural macro synthetic fibre. The specifications as found on the product data sheet are presented in Table 6.2 below. The fibre is supplied in kraft bags with 2.5kg of fibre per bag. Figure 7.5 shows a bag of BarChip 48 fibre as supplied.

Characteristic	BarChip 48	Standard
Fibre Class II	For structural use in concrete, mortar and grout	EN 14889-2
Tensile Strength	640 MPa	JIS L 1013/ISO2062
Young's Modulus	12 GPa	JIS L 1013/ISO2062
Length	48mm	
Anchorage	Continuous Embossing	
Base Material	Virgin Polypropylene	
Alkali Resistance	Excellent	
CE Certification		0120-GB10/79678
ISO 9001:2008 Certification		JKT0402914

Table 7.2 Specifications of BarChip48 after (BarChip., 2018)



Figure 7.5 Image of the BarChip 48 fibre as supplied.

7.8 Mix Design

7.8.1 Mix details

The mix design was designed as a C50 /60 concrete with a slump of 200mm and a maximum aggregate size of 16mm. There were three types of aggregate namely 8mm-16mm, 4mm-8mm and the sand classified as 0mm-4mm all shown in figures 7.6 – 7.8 along with their respective particle size distribution. All aggregates were locally sourced and uncrushed or natural. An initial sieve analyses showed the aggregates had insufficient fines and therefore it was decided to use crushed limestone as a filler shown in figure 7.9. The concrete was reinforced with a dose rate of 7kg per m³ of Barchip48 macro synthetic fibre which was added to the mix. The actual fibre is shown in Figure 7.10 along with a particle distribution of all the aggregates alongside each other. The cement was an OPC CEM1 42.5R supplied by Holcim under the name of Extracem shown in figure 7.11 and the superplasticizer used was Mapei Dynamon NRG 1020.

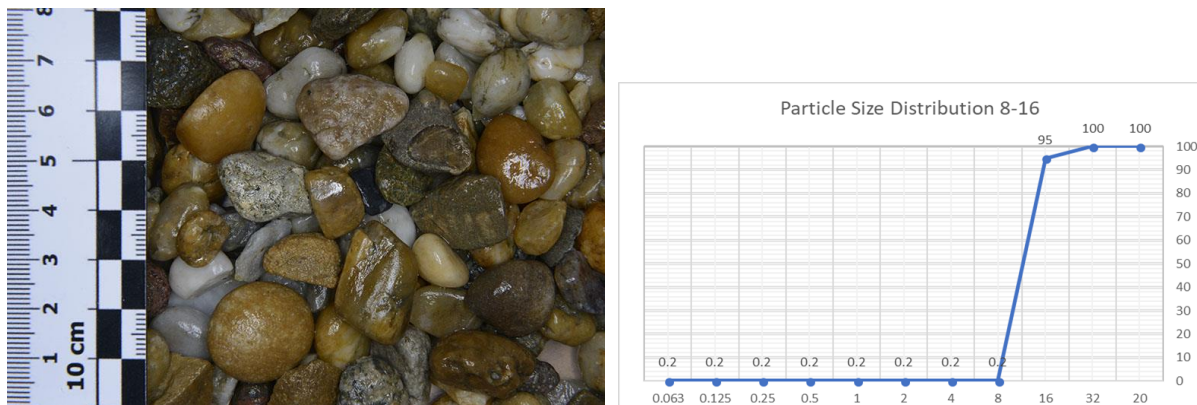


Figure 7.6 showing the 8-16mm Aggregate and the particle size distribution

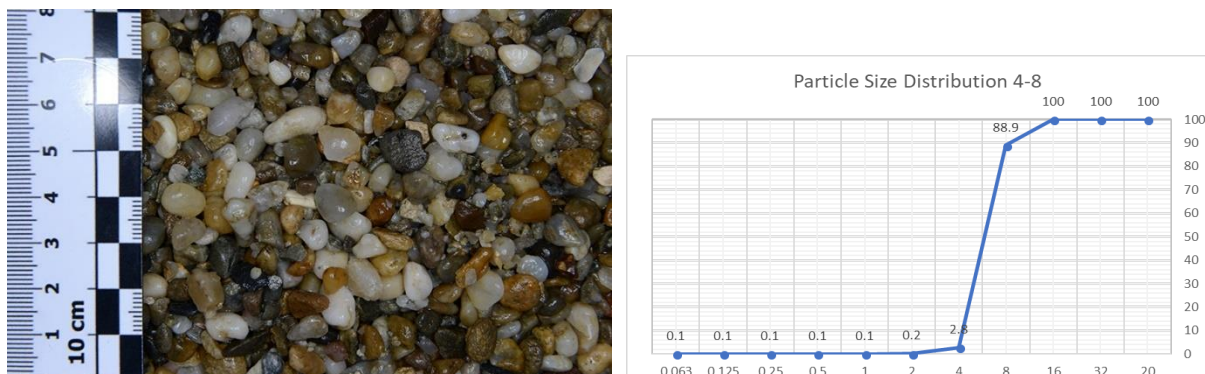


Figure 7.7 showing the 4-8 mm Aggregate and the particle size distribution

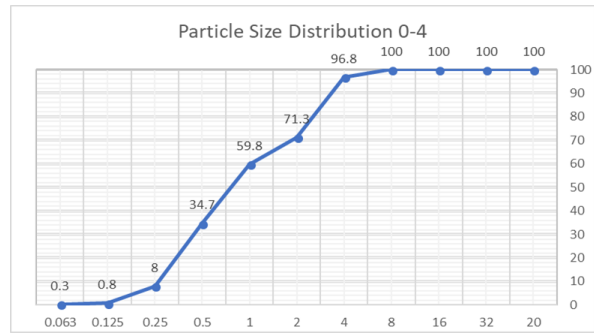
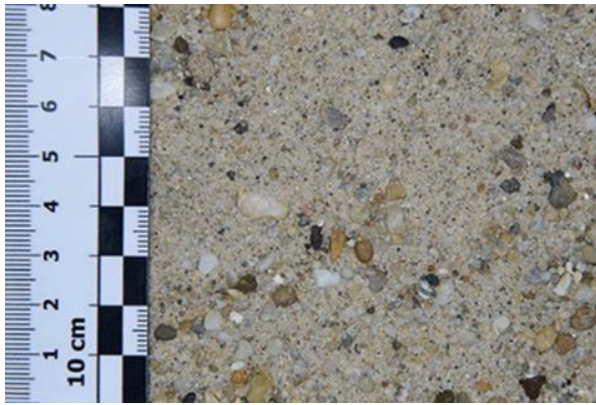


Figure 7.8 showing the 0-4mm Aggregate and the particle size distribution

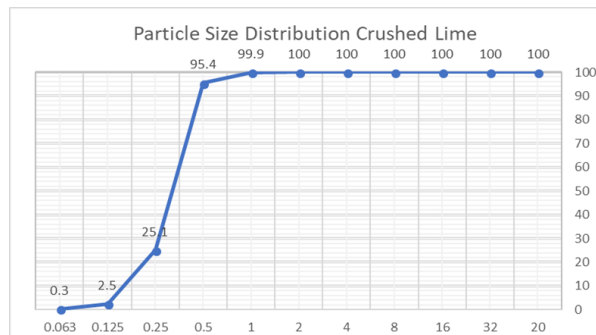
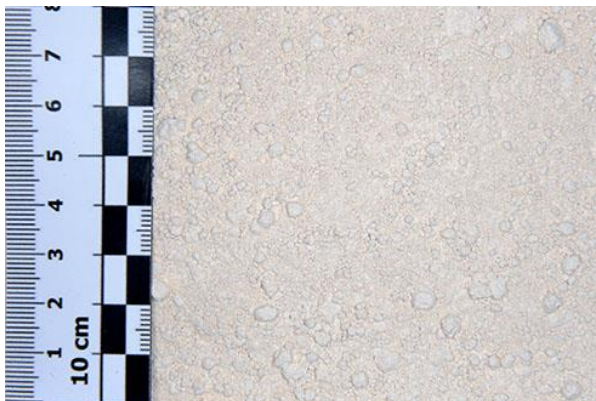


Figure 7.9 showing the crushed limestone and its particle size distribution

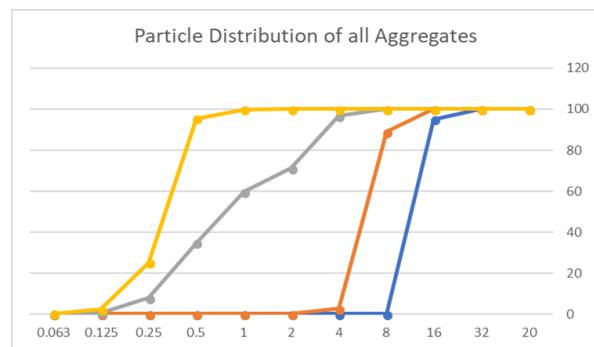
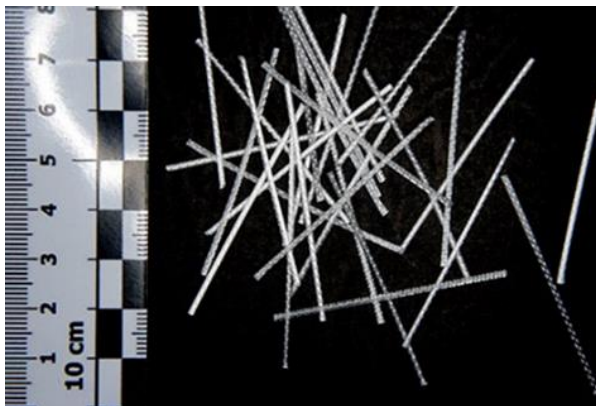


Figure 7.10 showing the BarChip48 fibre and particle distribution of all the aggregates



Figure 7.11 Showing the cement used in the mix as supplied.

7.8.2 Mix proportioning

Based on the sieve analysis a combined aggregate grading curve was plotted as shown in figure 7.12 and the aggregates were proportioned using the EN1766:2000 Grading curve for aggregates $D_{max}=16-20\text{mm}$

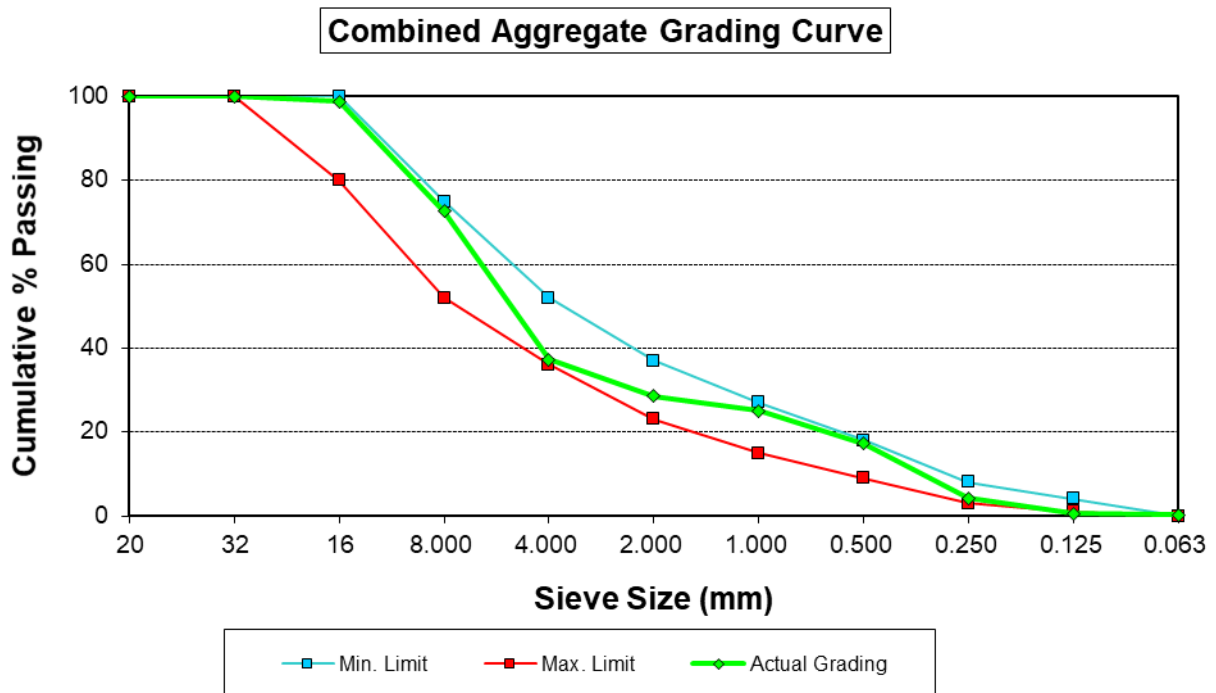


Figure 7.12 Showing the combined aggregate grading and the EN 1766:2000 grading curve.

The mix proportion for 1 m^3 is shown below in Table 7.2 The mixing was completed in the laboratory mixer. This did require a number of mixes which is not always ideal for

a size effect experiment but extra care was taken to ensure each mix was consistent with accurate measurement of the constituents and mixed under laboratory conditions.

Constituents	SG	Batch Weights	Volume
Cement	3.15	350	111
Water	1	170	170
8-16 Aggregate	2.64	428	162
4-8 Aggregate	2.64	744	282
0-4 Aggregate	2.64	558	211
Limestone powder	2.62	130	50
Superplasticizer	1.1	2	2
Barchip48 fibre	0.9	7	8
Air	1%	0	10
Total		2389	1006

Table 7.2 Showing mix proportioning used in the experiment

Slump measurements were taken and were a consistent 200mm +/- 10 and the air content measured was 6%, using the air metre. All moulds were filled and compacted on the vibrating table to ensure uniform compaction. Three cubes were cast to check the 28 day compressive strength and 1 cylinder was cast to measure the Young's Modulus which was 42.4 GPa. The 28 day calculated compressive strength is shown in Table 7.3 below.

	Weight g	A mm	B mm	Force Kn	UCS Mpa
Cube1	8166	150.62	151.03	1502	66.03
Cube2	8070	148.82	150.49	1537	68.63
Cube3	8072	151.47	150.76	1540	67.44
Mean	8102.67	150.30	150.76	1526.33	67.36
COV %	0.7	0.9	0.2	1.4	1.9

Table 7.3 Showing the uniaxial compressive strengths of the cubes at 28 days

7.9 Test Setup

7.9.1 Crack width measurement

The testing was performed in a Zwick/Roell Z150 with a 150kn capacity. The beams were loaded at a loading rate of 0.2mm / minute. The load and deflection of the piston was automatically recorded by the machine. The crack openings were all recorded manually using a mechanical dial gauge crack width monitor as shown in figure 7.13. The dial measures to an accuracy of 0.002 mm but with a maximum displacement of only 2.8 mm. Special machined brass grommets each with 2 measuring points are glued in place on the beams. The crack widths in the large beams were expected to exceed the maximum displacement of the gauge which is why the brass grommets each had two measuring points machined as shown in figure 7.14. The initial measurements at crack propagation were taken with the two external measuring points and as the crack opened an outer and inner point was used and finally the two inner points.



Figure 7.13 Showing the mechanical dial gauge crack width monitor.

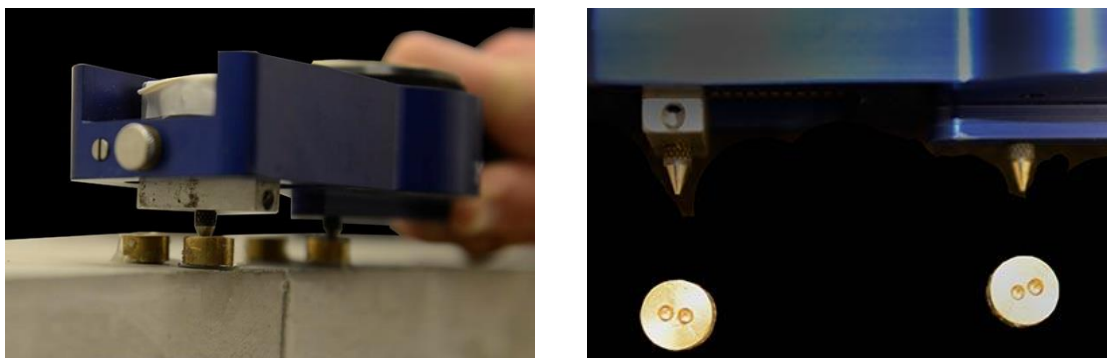


Figure 7.14 showing the brass grommets and pins under the crack width monitor and measurement details.

The brass grommets were placed on the beams on either side of the notch / expected crack propagation path as shown in figure 7.15. With measuring points at the crack mouth (bottom of the notch at base of beam), Crack tip, (top of notch) and then for the large and medium beams at two equally spaced points between the top of the notch and the top of the beam as show in figure 7.16, while the small sized beams had one measuring point centrally located between the top of the notch and the top of the beam. On five of the fibre reinforced standard beams measuring points were only placed at the top and bottom of the notch. While on two of them an additional measuring point was placed between the top of the notch and the top of the beam. All the actual measurements taken are shown in Appendix 1.



Figure 7.15 showing positioning of the brass grommets.

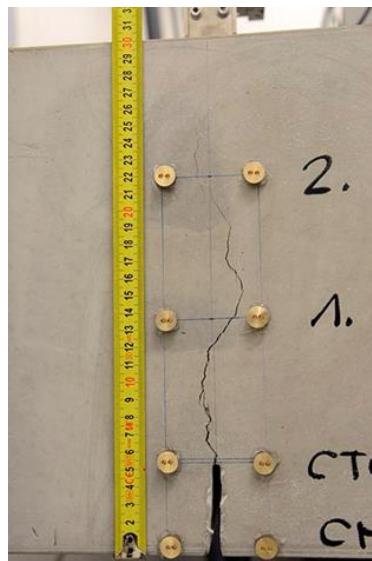


Figure 7.16 showing the in-situ configuration of the measuring points on the large beam, The tape is there purely for scale.

Chapter 8 Results and Discussion

8.1 Large beams

Three large beams as previously discussed measuring 300mm x 300mm with a length of 1050mm were cast. They were rotated 90 degrees around their longitudinal axis and a notch of planned 50mm was wet sawn through the width at mid span. but were tested at span of 1000mm. The beams are identified as L01, L02 and L03, the actual notch depths were 50.31, 50.23 and 50.83mm respectively. A large beam without fibre was also cast but unfortunately the mould deformed and the beam was abandoned. Figure 8.1 shows the first beam set in the testing machine prior to testing and figure 8.2 shows the beam at the conclusion of the test,

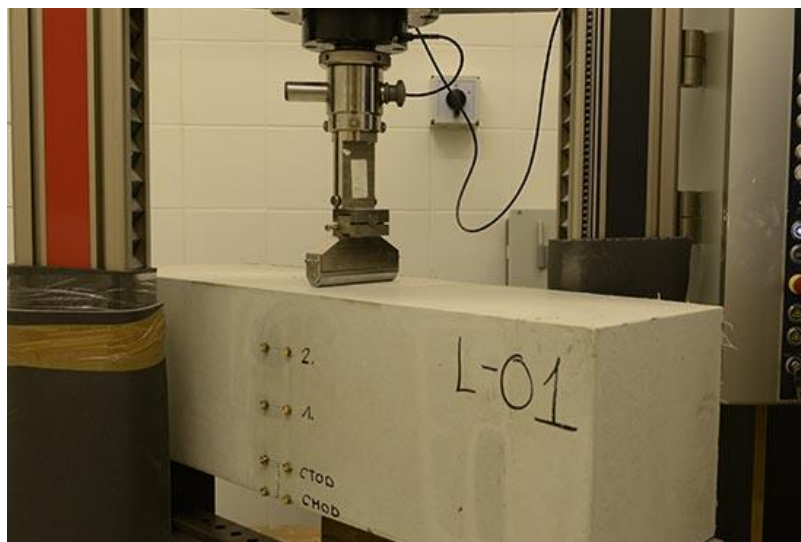


Figure 8.1 Showing the first large beam in place at start of test.

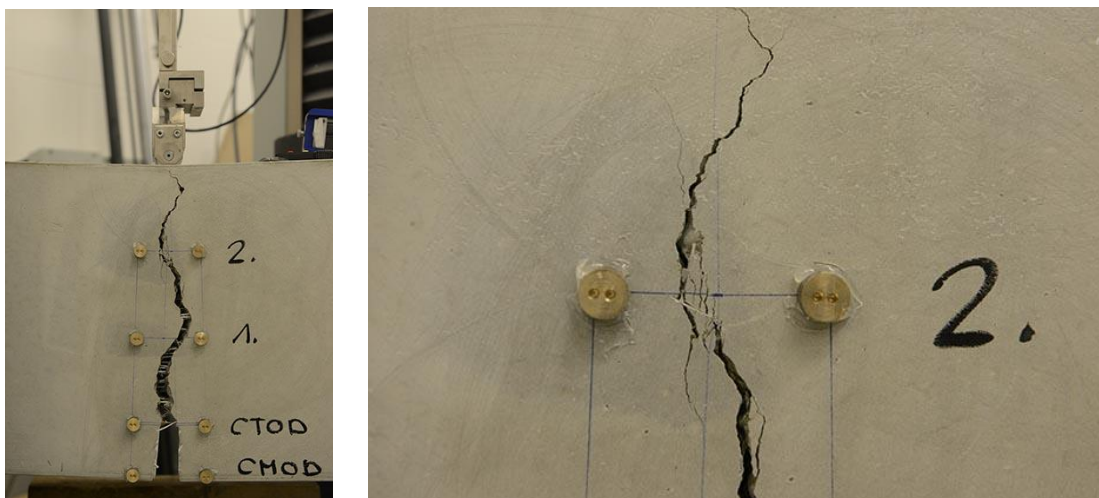


Figure 8.2 showing the first large beam at conclusion of test and a close up of the crack showing branching.

It is interesting to note how there is one major crack which tended to branch out towards the end of the test. All three beams showed post crack hardening. The test was concluded once 15mm CMOD was measured, at this point none of the beams had totally failed. Figure 8.3 shows the load deformation curves and the load – CMOD diagram showing F_{max} (Limit of proportionality) and $CMOD_{1-4}$ measured at CMOD 0.5, 1.5, 2.5 and 3,5mm respectively. The summary of results is tabulated in Appendix 2. The large beams had four measuring points which were measured at each mm of downward deflection. The crack distance from the top of the beam was also measured at the same time. Additional measurements on Beam L02 and Beam L03 were also taken at the end of the test once the load had been removed.

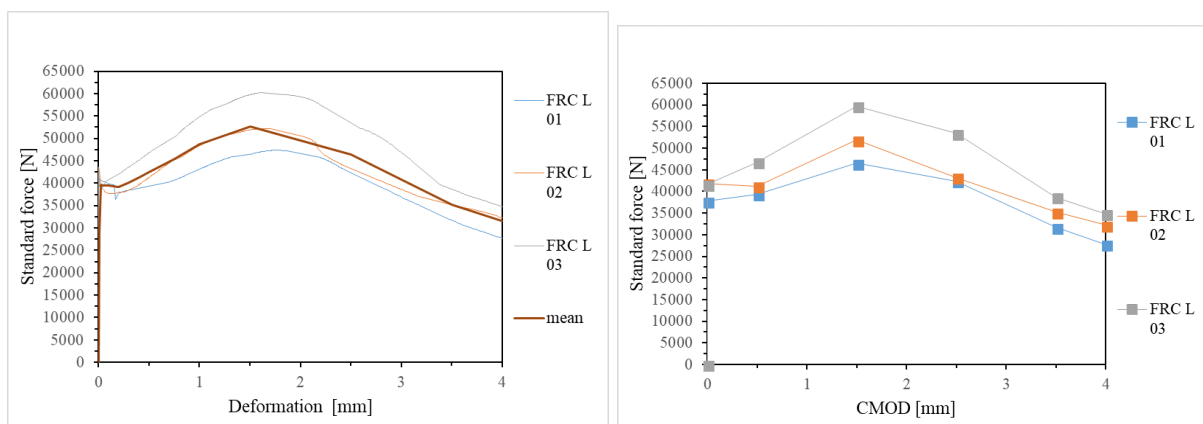


Figure 8.3 showing the load deformation and load -CMOD diagram for the three large beams.

8.2 Medium beams

Three medium beams as previously discussed measuring 225mm x 300mm with a span of 700mm were cast. The beams were rotated 90 degrees around their longitudinal axis and a notch of planned 37.5 mm was wet sawn through the width at mid span. The beams are identified as M01 (Plain concrete), M02, M03 and M04, the actual notch depths of the fibre reinforced beams were 38.9, 38.2 and 36.6mm respectively. Figure 8.4 shows the first beam set in the testing machine prior to testing showing the four measuring points across the potential crack. On beam MO4 the top measuring point as lost after 2mm of deflection, when the crack deflected right as shown in figure 8.5. which shows a comparison between two beams where one the crack misses the predicted path while in the other image the crack follows the centre

line almost perfectly. Figure 8.6 shows the load displacements and load CMOD results of all three fibre reinforced beams.



Figure 8.4 showing a medium beam ready for testing.

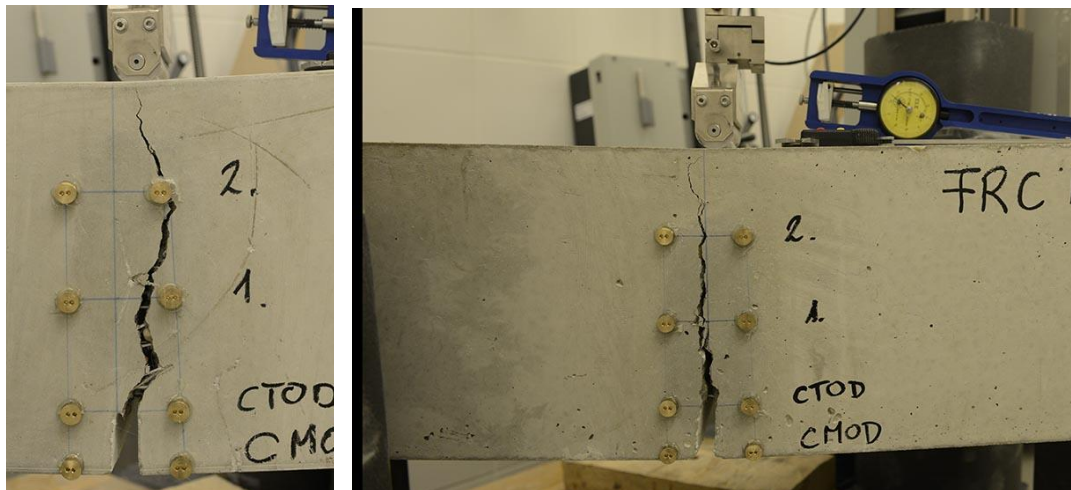


Figure 8.5 showing the unpredictability of a crack, the left hand image the crack misses the measuring point while on the right the crack is near perfect central.

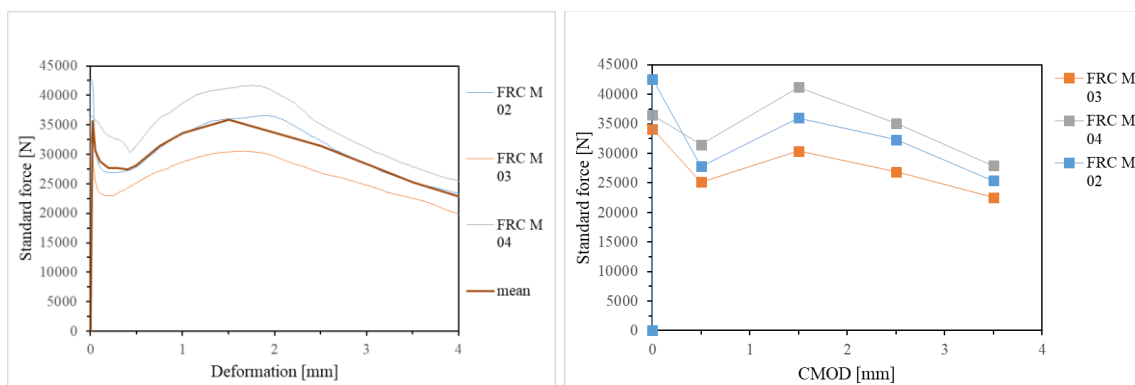


Figure 8.6 Load deformation and load CMOD results for the medium sized beams

8.3 Small beams

Four small beams as previously discussed measuring 150mm x 300mm with a span of 500 mm were cast. Three of them were reinforced with macro synthetic fibre while the fourth beam was plain concrete. The beams were rotated 90 degrees around their longitudinal axis and a notch of planned 25 mm was wet sawn through the width at mid span. The beams are identified as S01, S02, S03 and S04, the actual notch depths of the fibre reinforced beams were 26.5mm, 24.3mm and 28.9mm respectively. Figure 8.7 shows the first beam set in the testing machine prior to testing, while the righthand image shows the setup of the measuring points. Figure 8.8 shows the load deformation and load CMOD graphs of the three fibre reinforced small beams.

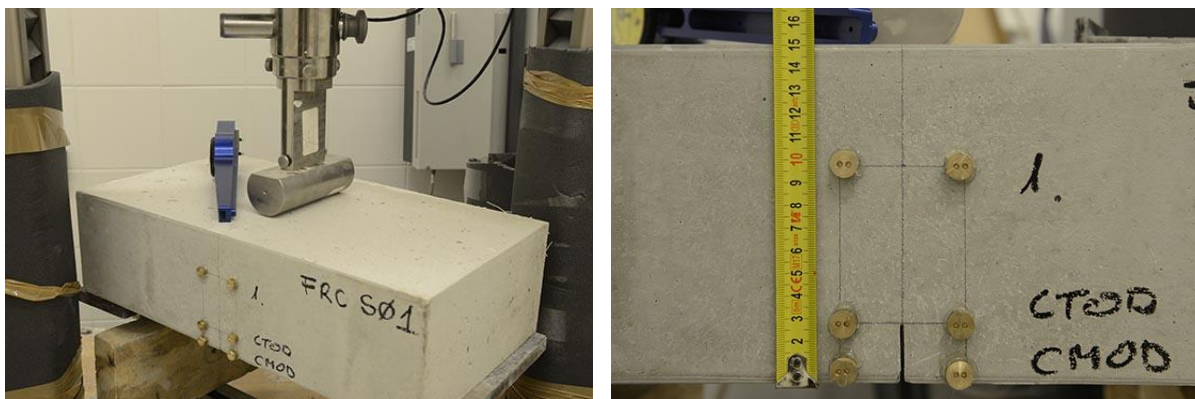


Figure 8.7 Showing the first small beam ready for testing and on the right the setup of the measuring points.

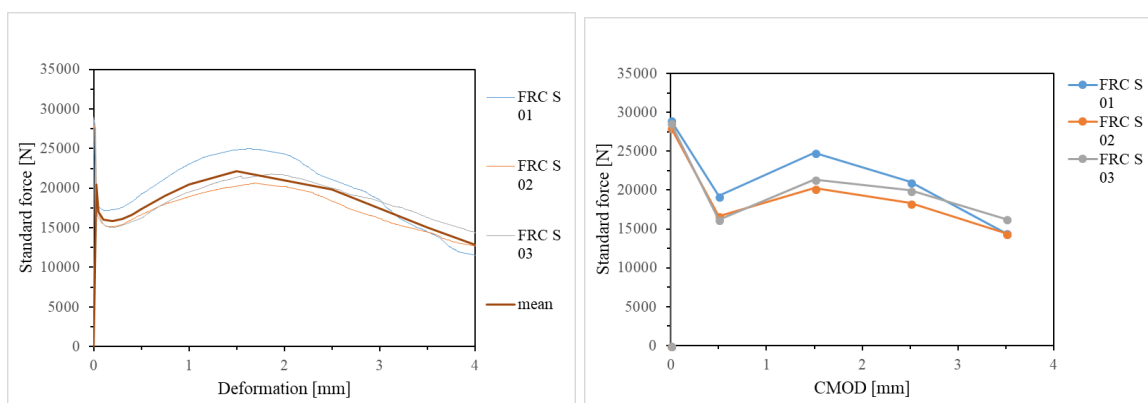


Figure 8.8 Showing the combined load deformation and load CMOD graphs for the small beams.

8.4 Standard Beams

A total of ten standard beams as previously discussed measuring 150mm x 150mm with a span of 500 mm were cast. Seven of them were reinforced with macro synthetic fibre while the final three were plain concrete. The beams were rotated 90 degrees around their longitudinal axis and a notch of planned 25 mm was wet sawn through the width at mid span. The average notch depth across the beams was 26.96mm. Of the seven standard beams reinforced with synthetic fibre, the first 5 beams had only a CMOD and CTOD measuring station, the final two beams has an additional measuring station as shown in figure 8.9. Figure 8.10 shows the first beam set in the testing machine prior to testing. Figure 8.11 shows the load deformation and load CMOD graphs of the seven fibre reinforced small beams.

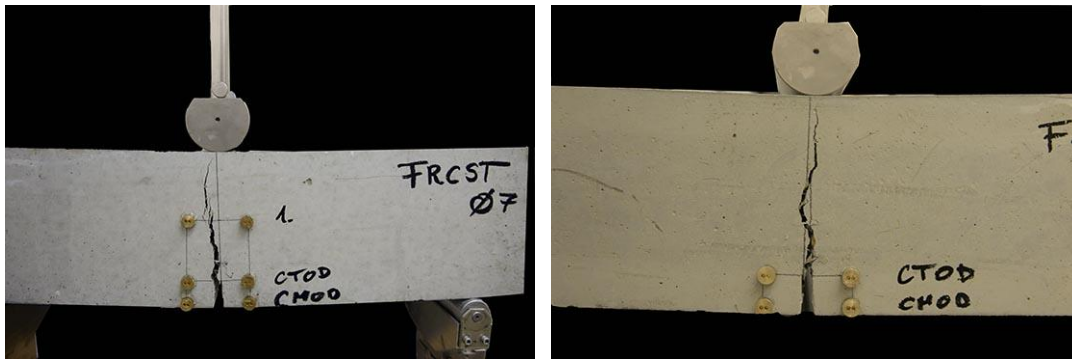


Figure 8.9 showing the measuring stations for beam 06 & 07 on the left and the other five beams on the right.



Figure 8.10 Showing a standard beam at the start of a test.

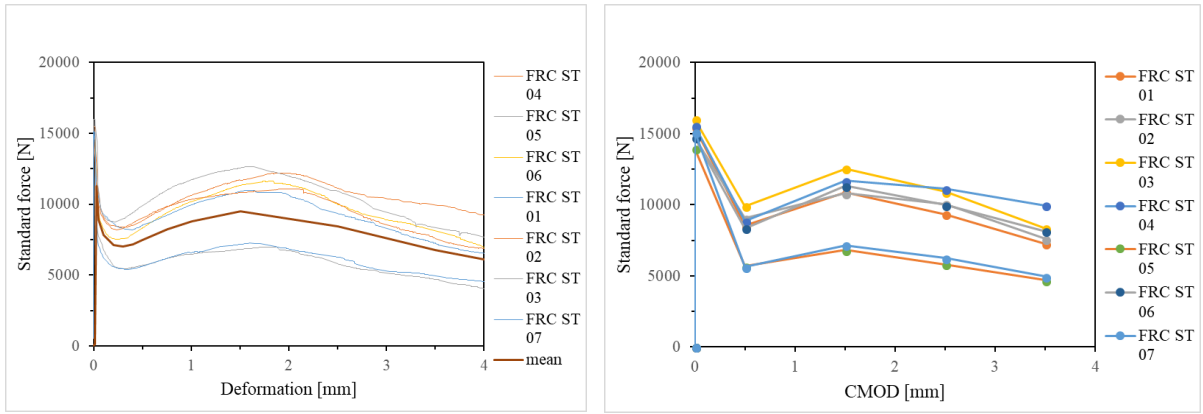


Figure 8.11 Showing the combined load deformation and load CMOD graphs for the standard beams.

8.5 Comparison of beam results.

8.5.1 Load – CMOD

The load measured in Newtons compared to the crack mouth opening displacement, measured in mm is represented graphically in figure 8.12 with the summary of results tabulated in Appendix 2. This representation compares the entire data set of all the fibre reinforced concrete beams being three large, three medium, three small and seven standard beams. The comparison of the mean of each set of beams is shown graphically in figure 8.13. Full summaries of the comparative results showing both loads and force is given in Appendix 2.

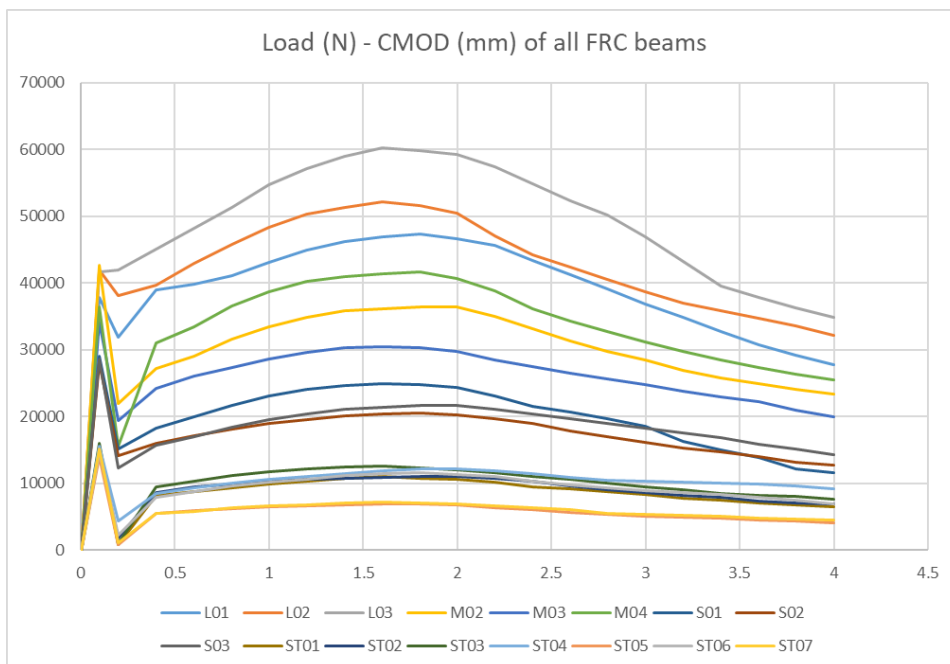


Figure 8.12 Showing the load (N) and CMOD (mm) of all the FRC Beams tested.

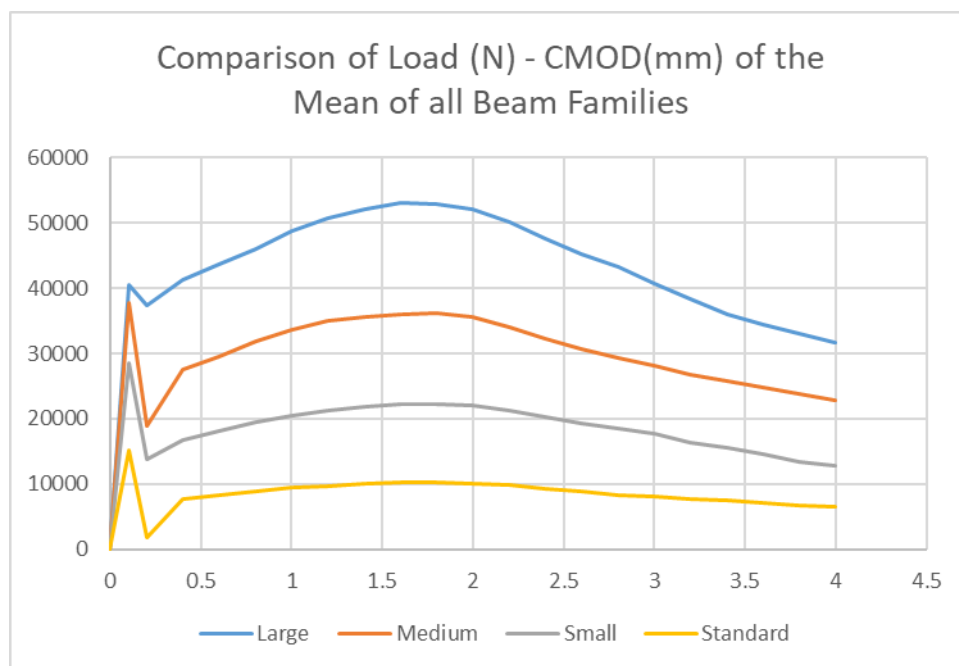


Figure 8.13 showing the mean of the load (N) – CMOD (mm) of the different beam sets tested.

8.5.2 Residual flexural tensile strength

The calculated residual strengths, measured in megapascals, compared to the crack mouth opening displacement, in millimetres, is represented graphically in figure 8.14 with the summary of results tabulated in appendix 3. This representation compares the entire data set of all the fibre reinforced concrete beams being three large, three medium, three small and seven standard beams. The comparison of the mean of each set of beams is shown graphically in figure 8.15.

The actual values for each point on the graph in Figure 8.15 is given in table 8.1. The values in the table are all expressed to the nearest 0.1 N/mm². The most obvious observation is that the smaller the beam the larger the F_L value but once the concrete has cracked this trait is reversed and the larger the beams the higher the CMOD_j values are where (j = 1,2,3,4).

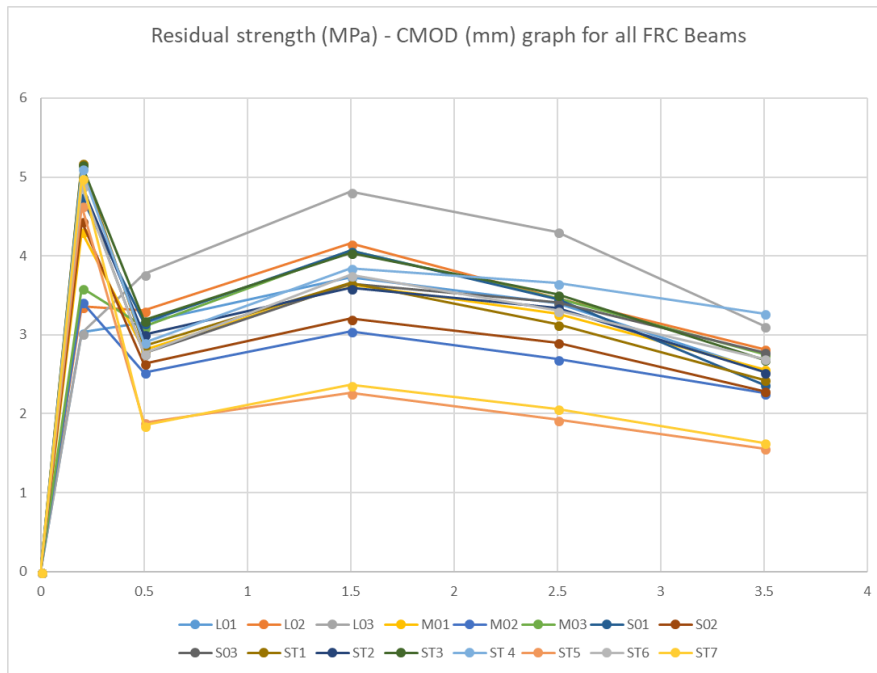


Figure 8.14 Showing a graphical representation of the load – CMOD diagram of all the FRC Beams tested

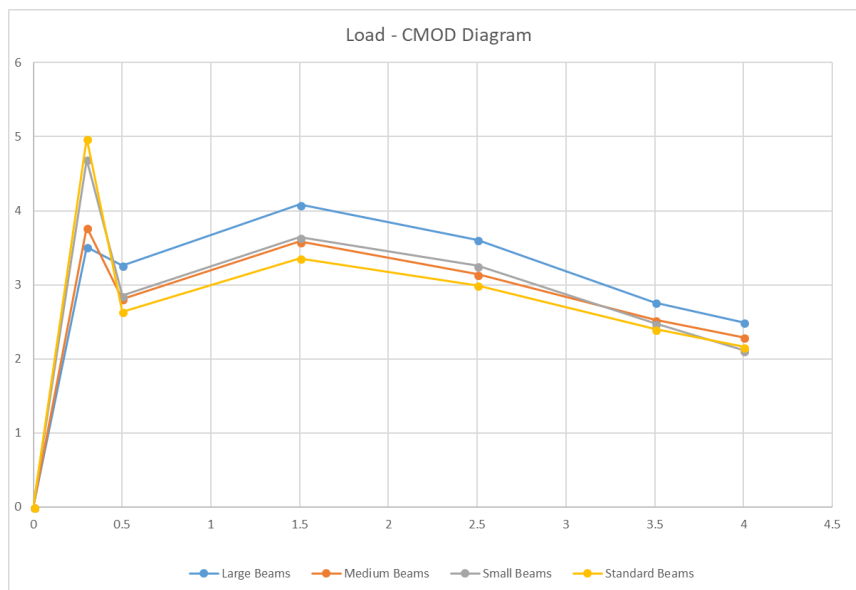


Figure 8.15 showing the mean combined average load – CMOD diagram for each set of beams

Beams	F_L	CMOD ₁ 0.5	CMOD ₂ 1.5	CMOD ₃ 2.5	CMOD ₄ 3.5	4
Large	3.5	3.3	4.1	3.6	2.8	2.5
Medium	3.8	2.8	3.6	3.1	2.5	2.3
Small	4.7	2.9	3.6	3.3	2.5	2.1
Standard	5.0	2.6	3.4	3.0	2.4	2.2

Table 8.1 Showing the values in n/mm² for corresponding to the peak load F_L and CMOD_{1,2,3,4}

8.5.3 Introducing the Bazant size effect law into the data set.

The Bazant size effect law which essentially considers stress per unit area is not dissimilar to the residual strength calculations and graphically presents a very similar trend as shown in figure 8.16 which graphically plots the peak load and loads at the normal CMOD_(0.5, 1.5, 2.5,3.5) positions using equation 1.1. The full set of load and calculated results are tabulated in Appendix 3.

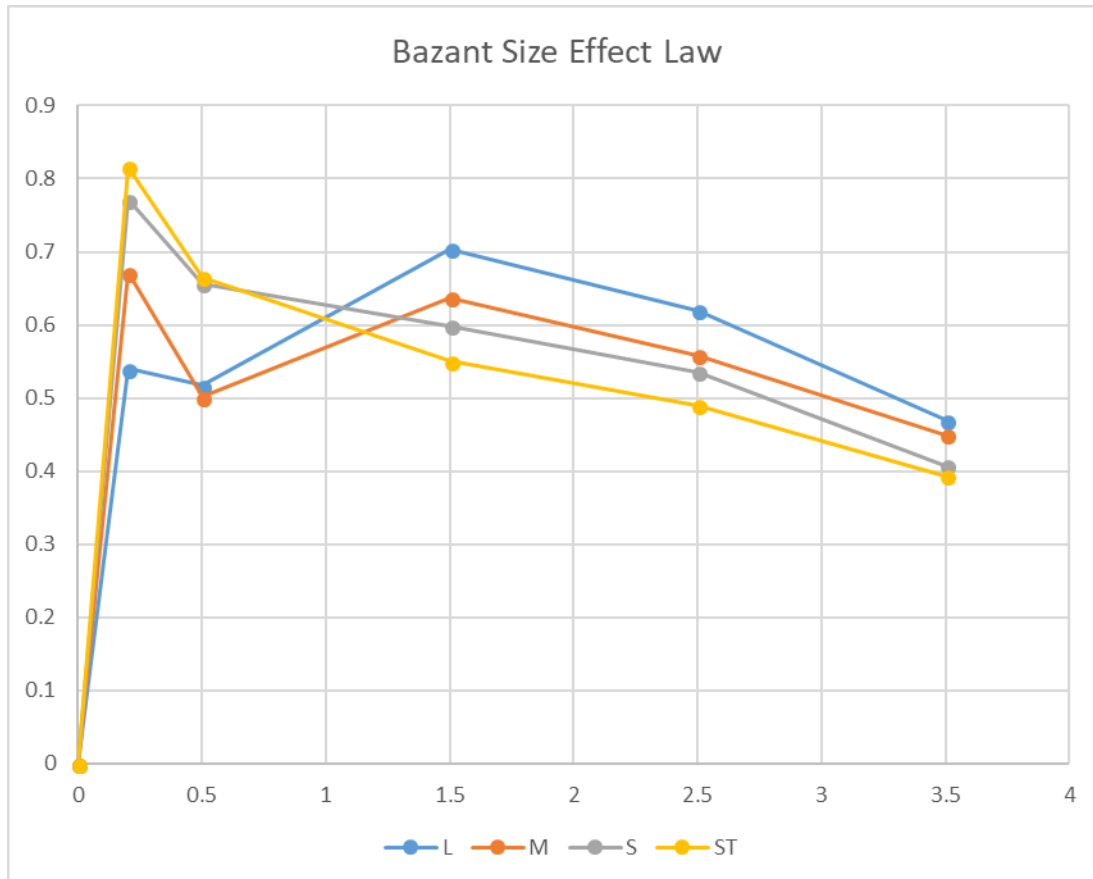


Figure 8.16 showing graphically the calculated Bazant values represented as a load – CMOD diagram.

8.5.4 Introducing the equivalent angle method of calculating size effect.

To determine if there is a size effect when testing geometrically similar prisms the rotational angle should remain constant to simplify the calculation. Varying the depths and spans of the beams will alter the rotational angle for a similar CMOD as shown in figure 8.17. The equivalent angles of the three size beams were determined as shown in table 8.2. The large beams have the same rotational angle at 2mm deflection as

the small beams have at 1mm deflection. The standard beams being the same height depth and span as the small beams have the same rotational angle at the same deflection.

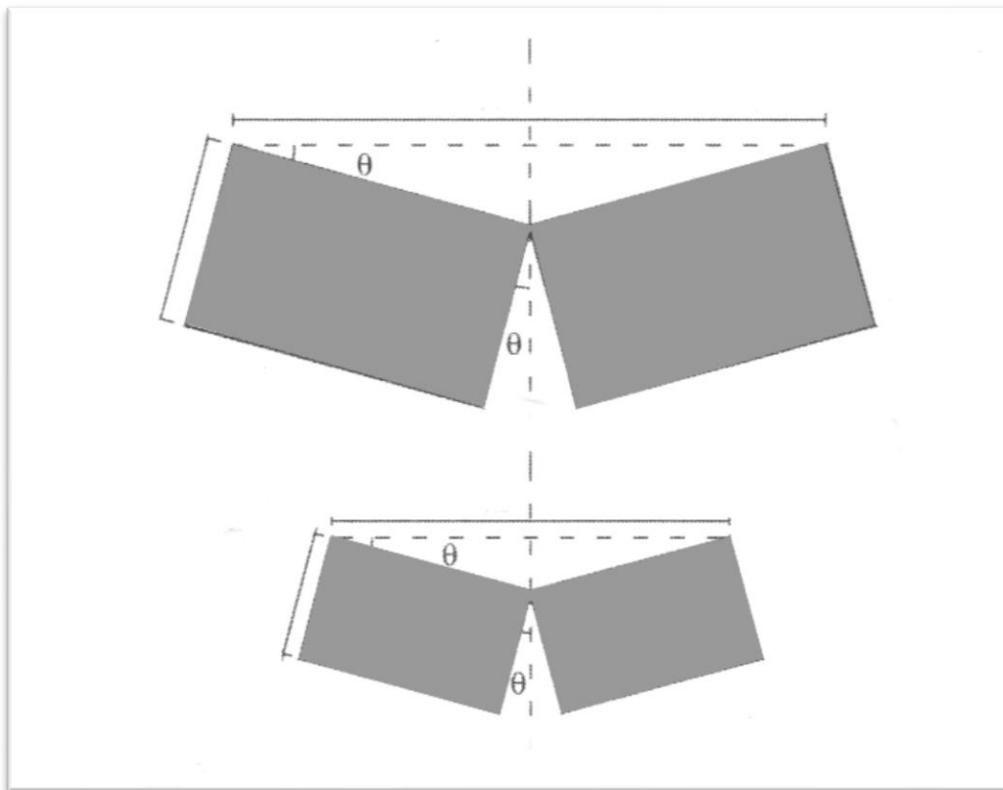
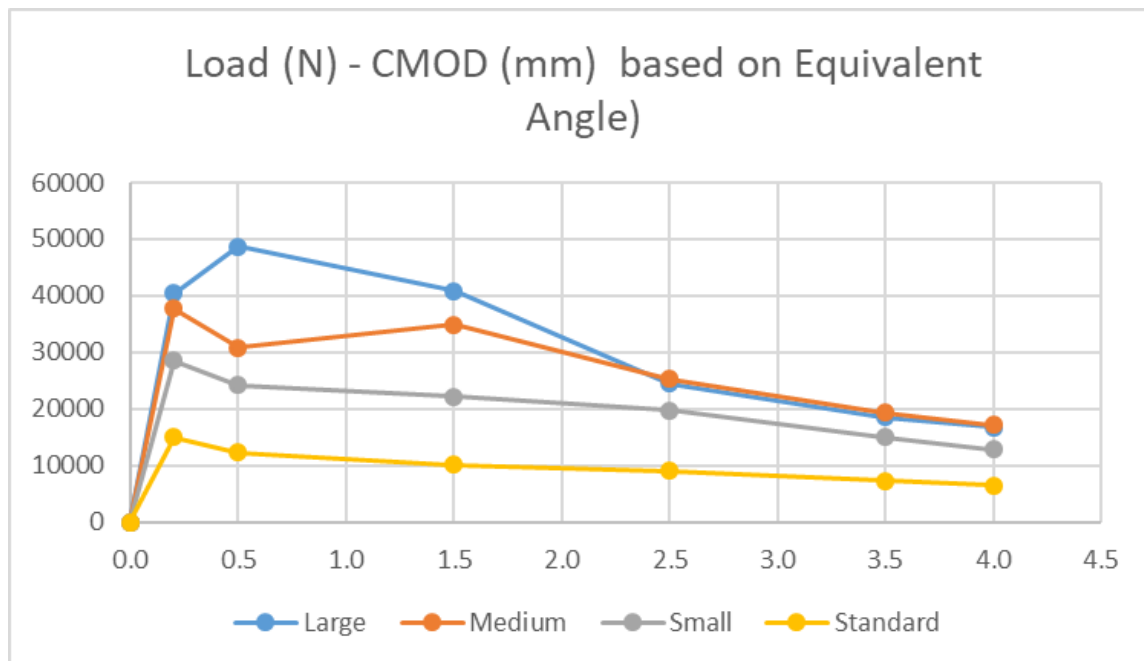


Figure 8.17 showing how the deformation varies for the same rotational angle.

Equivalent Deflections (mm)		
Large	Medium	Small
1	0.7	0.5
2	1.4	1
3	2.1	1.5
4	2.8	2
5	3.5	2.5
6	4.2	3
7	4.9	3.5
8	5.6	4
9	6.3	4.5
10	7	5

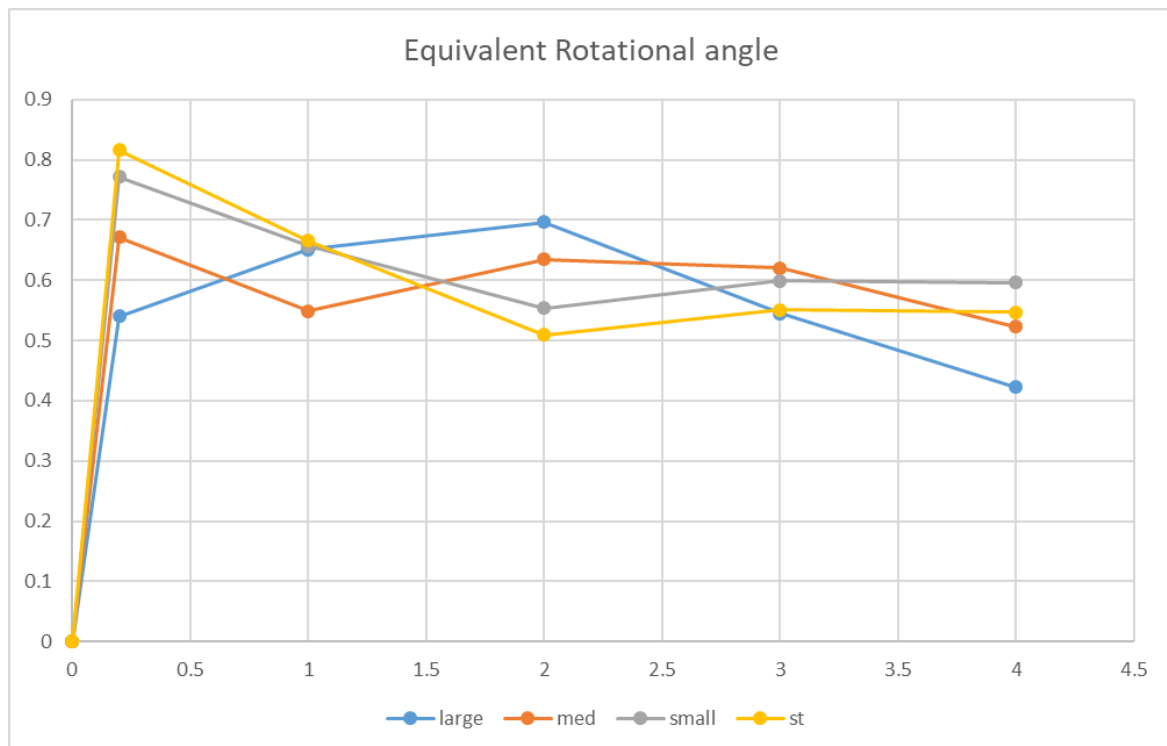
Table 8.2 showing the deflections in mm required to get the same rotational angle of the three beam sizes

By matching the loads to the new deflections and then representing this graphically the graph shown in figure 8.18 was produced with the data points tabulated below. Using Bazants size effect equation the new results are shown both graphically and in tabulated form in figure 8.19 The graphs are truncated at a CMOD of 4mm which was realistically 8mm CMOD for the large beam and 5.6mm CMOD for the medium sized beam. The full set of load and calculated forces are tabulated in Appendix 4.



Summary Load in Newtons / Equivalent Angles of Deformation							
		fMax	f1 (0.5)	f2 (1.5)	f3 (2.5)	f4 (3.5)	4
	0.0	0.2	0.5	1.5	2.5	3.5	4.0
Large	0	40454.52	48716.21	40796.58	24477.03	18530.66	16720.57
Medium	0	37725.72	30843.31	34869.21	25277.02	19402.88	17148.6
Small	0	28560.14	24232.64	22152.82	19804.38	15071.07	12864.26
Standard	0	15074.29	12289.14	10182.89	9066.126	7275.581	6551.203

Figure 8.18 Showing graphically and numerically the results when the rotational angle is equalised between the beams.



	Peak	1	2	3	4
large	0.54039	0.650796	0.696644	0.54501	0.422174
med	0.671159	0.548464	0.634579	0.620054	0.522512
small	0.771693	0.656683	0.553568	0.598636	0.595846
st	0.815761	0.665201	0.509026	0.550813	0.54735

Figure 8.19 Showing graphically and numerically the results after the original loads are calculated into forces using Bazant's size effect equation.

8.5.5 Discussion

The main aim of this project was to compare the results of the geometrically similar prisms of different sizes to determine if there is a size factor at work in macro synthetic fibre reinforced prisms.

With the large beams which measured 300mm x 300mm x 1000mm, there was post crack hardening. This is not normally seen with smaller beams, the notch essentially limited the beams to a single crack, although as the crack propagated towards the top branching was evident. The question is, would multiple cracking occur if it was a unnotched beam, which is what one would expect with post crack hardening. Monitoring of the four measuring stations showed in the early stages a definite compression zone towards the top of the beam.

The plain concrete beams behave as would be expected with failure very soon after the initial crack and limited information was obtained from these tests. Although they did confirm a size effect.

When the different beams are compared together regardless of if Bazants equation is used, the LOP equation or equivalent rotational angles coupled with Bazants equation the one obvious thing is that up to the point of the first crack there is definitely a size effect at work. This is a result that was to be expected.

What is more interesting is that after the crack there is a build-up of load carrying performance by the fibres and these do not reflect size effect, but the totally opposite, as while the large beams performance in terms of force (MPa) is the worst pre-crack, post crack it performs the best regardless of how it is analysed.

When comparing the standard beams measuring 150mm x 150mm with a 25mm notch to the small beams measuring 150mm x 300mm (Wide) with a 25mm notch. The main observation was that the additional width reduced the coefficient of variability by half but the size effect only reduced the residual strength at first crack by an average of 6 % and the fibres giving an increase of 9 % residual strength at CMOD1.5 and CMOD2.5. with increasing depth of beam the peak residual strength reduced to 76% and 63% respectively for the medium sized and large sized beams . The opposite as discussed occurring post crack where the fibres increase the residual strength with an increase of beam depth and width by 116% and 128% respectively for the medium and large beams at the same CMOD points.

It should be noted that this experiment was based on a small data set but it certainly shows a trend that with increased size while the first crack peak strength reduces the post crack residual strength produced by the inclusion of macro synthetic fibre increases.

The question does arise as to is there a cut off point of this increased residual strength with increased size and also warrants the question of, if a standard beam

test truly represents the increased ductility with size that macro synthetic fibre produces.

To reiterate the coefficient of variation (COV) the general observation which was no surprise was that while it was particularly high in the standard beams with COV of typically 20% this seemed to half with wider beams of the same height but with increased height there seemed little difference.

Chapter 9 Conclusions

The coefficient of variation in the testing reduces with the increase in width of the beams with the 300mm beams showing half the percentage of variation compared to the standard 150mm beams of the same height.

Increasing the depth of the beams did very little to change the Coefficient of variation in the testing comparing beams of 300mm width and different depths.

The addition of Barchip 48 macro synthetic fibre at an acceptable dose rate can change the post crack response of concrete from brittle to ductile behaviour.

In thick sections post crack hardening can be achieved with macro synthetic fibre, this is obviously fibre type and dosage dependant.

Size effect is very real in plain concrete as well as in macro synthetic fibre reinforced concrete until the peak strength is reached and the section cracks. Once cracked there is no longer a size effect with the load carrying capacity of the cracked section of fibre reinforced concrete increasing relative to size.

There is certainly a need for additional research in this area to determine the full effect of macro synthetic fibres post crack performance, especially in realistic sized beams where there is minimal effect of boundary conditions and fibre alignment.

Further research could not only increase the confidence level in the above observations but could also determine what is probably a hyperbolic residual strength increase with increased depth and determine the suggested hyperbolic curve of depth to strength increase.

References

- ACI. 1991. *ACI 446.1R-91 Fracture Mechanics of Concrete: Concepts, Models and Determination of Material Properties*. USA: American concrete Institute.
- ACI. 2018a. *ACI 544.4R-18 Guide to Design with Fiber-Reinforced Concrete*. Farmington Hills: American Concrete Institute.
- ACI. 2018b. *ACI Concrete Terminology ACI-CT18*. March 2018 ed. Farmington: ACI.
- Amin, A., Foster, S.J., Gilbert, R.I. and Kaufmann, W. 2017. Material characterisation of macro synthetic fibre reinforced concrete. *Cement and Concrete Composites*. **84**, p10.
- Amin, A., Foster, S.J. and Muttoni, A. 2015. Derivation of the σ -w relationship for SFRC from prism bending tests. *Structural Concrete*. **16**(1), pp.93-105.
- ASTM. 2010. *ASTM C1550-10a Standard Test Method for Flexural Toughness of Fiber Reinforced Concrete (Using Centrally Loaded Round Panel)*. West Conshohocken: ASTM.
- ASTM_C_1609. 2012. *ASTM C 1609 2012, Standard test method for flexural performance of fiber reinforced concrete* ASTM.
- Babafemi, A.J. and Boshoff, W.P. 2017. Pull-out response of macro synthetic fibre from concrete matrix: Effect of loading rate and embedment length. *Construction and Building Materials*. **135**, p10.
- Bakhshi, M., Barsby, C. and Mobasher, B. 2014. Comparative evaluation of early age toughness parameters in fiber reinforced concrete. *Materials and Structures*. **47**, p20.
- Balaguru, P.N. and Shah, S.P. 1992. *Fibre Reinforced Cement Composites*. USA: McGraw-Hill.
- BarChip. 2018. *BarChip48 Product Data Sheet (PDS)*. [Leaflet]. Australia.
- Bazant, Z.B. and Planas, J. 1998. *Fracture and Size Effect in concrete and other quasibrittle materials*. USA: CRC Press LLC.
- Bazant, Z.P. 2002. Concrete fracture models: testing and practice. *Engineering Fracture Mechanics*. **69**, pp.165-205.
- Bazant, Z.P. and Kazemi, M.T. 1990. Determination of fracture energy, process zone length and brittleness number from size effect, with application to rock and concrete. *International journal of fracture*. **44**, pp.111-131.
- Bernard, E.S., Xu, G.G. and Carino, N.J. 2010. Influence of the number of replicates in a batch on apparent variability in FRC and FRS performance assessed using ASTM C1550 panels. In: Bernard, E.S., ed. *Shotcrete Elements of a system, Queenstown, New Zealand*. Leiden: Taylor & Francis Group, p.10.
- Beygi, M.H., Kazemi, M.T., Nikbin, I.M., Amiri, J.V., Rabbanifar, S. and Rahmani, E. 2014. The influence of coarse aggregate size and volume on the fracture behaviour and brittleness of self compacting concrete. *Cement and Concrete Research*. **66**, p15.
- Beygi, M.H.A., Kazemi, M.T., Nikbin, I.M. and Amiri, J.V. 2013. The effect of water to cement ratio on fracture parameters and brittleness of self compacting concrete. *Materials and Design*. **50**, p10.
- BSI. 2006a. *BS EN14488-3:2006 Testing sprayed concrete- Part 3: Flexural strengths (first peak, ultimate and residual) of fibre reinforced beam specimens*. London: BSI.
- BSI. 2006b. *BS EN14488-5:2006 Testing sprayed concrete- Part 5: Determination of energy absorption capacity of fibre reinforced slab specimens*. London: BSI.
- BSI. 2006c. *BS EN 14889-1:2006 Fibres for concrete part 1 Steel fibres — Definitions, specifications and conformity*. London: BSI.
- BSI. 2006d. *BS EN 14889-2:2006 Fibres for concrete Part 2: Polymer fibres — Definitions, specifications and conformity*. London: BSI.
- BSI. 2008. *BS EN 14651:2005+A1:2007 Test method for metallic fibre concrete-Measuring the flexural tensile strength (limit of proportionality (LOP), residual)*. London: BSI.

- Buratti, N., Mazzotti, C. and Savoia, M. 2010. Experimental study on the flexural behaviour of fibre reinforced concretes strengthened with steel and macro-synthetic fibres. In: *Fracture Mechanics of Concrete and Concrete Structures, 23 - 28 May 2010, Korea*. Korea Concrete Institute, pp.1286 - 1294.
- Conforti, A., Minelli, F., Plizzari, G.A. and Tiberti, G. 2017. Comparing test methods for the mechanical characterization of fiber reinforced concrete. *Structural Concrete*. **2017:1-14**.
- Day, K.W., Aldred, J. and Hudson, B. 2017. *Concrete Mix Design, Quality Control and Specification*. 4th ed. London: CRC Press.
- di Prisco, M., Colombo, M. and Dozio, D. 2013. Fibre-reinforced concrete in fib Model Code 2010: principles, models and test validation. *Structural Concrete*. **14(4)**.
- EFNARC. 2011. *Testing sprayed concrete - EFNARC three point bending test on square panel with notch* Switzerland: EFNARC.
- Erdem, E. 2003. The flexural behaviour of SFRC Beams and slabs bending with σ - ϵ method. In: *International RILEM Workshop on Test and Design Methods for Steel Fibre Reinforced Concrete - Background and Experiences*: RILEM, p.222.
- Fantilli, A.P., Chiaia, B. and Gorino, A. 2016. Fiber volume fraction and ductility index of concrete beams. *Cement and Concrete Composites*. **65**, p11.
- Fib. 2012. Model Code for Concrete Structures 2010 - Final draft. *Fib Bulletin no 65 and 66. Dialogues Concerning Two New Sciences*. 1638. [Online database]. <http://oll.libertyfund.org/titles/galilei-dialogues-concerning-two-new-sciences>.
- Giaccio, G., Tobes, J.M. and Zerbino, R. 2008. Use of small beams to obtain design parameters of fibre reinforced concrete. *Cement and Concrete Composites*. **30**, p10.
- Gribniak, V., Kaklauskas, G., Kwan, A.K.H., Bacinscas, D. and Ulbinas, D. 2012. Deriving stress strain relationships for steel fibre concrete in tension from tests of beams with ordinary reinforcement. *Engineering Structures*. **42**, p9.
- Hoek, E. and Brown, E.T. 1982. *Underground Excavations in Rock*. London: The Institution of mining and metallurgy.
- Hoover, C.G., Bazant, Z.P., Vorel, J., Wendner, R. and Hubler, M.H. 2013. Comprehensive concrete fracture tests: Description and results. *Engineering fracture mechanics*. **114**, pp.93-103.
- Irwin, G.R. 1957. Analysis of stresses and strains near the end of a crack traversing a plate. *Journal of Applied Mechanics*. **24**, p4.
- Jamet, D., Gettu, R., Gopalaratnam, V.S. and Aguado, A. 1995. Toughness of Fiber-Reinforced High-Strength Concrete from Notched Beam Tests. In: Stevens, D.J. ed. *Testing of Fiber Reinforced Concrete*. American Concrete Institute.
- Jamsawang, P., Suansomjeen, T., Sukontasukkul, P., Jongpradist, P. and Bergado, D.T. 2018. Comparative flexural performance of compacted cement-fiber-sand. *Geotextiles and Geomembranes*. **46**, p12.
- JCI-S-002. 2003. *JCI-S-002-2003 Method of test for load – CMOD curves for fibre reinforced concrete using notched beams*. . Japan: Japanese Concrete Institute Standard.
- JCI. 2003. *JCI-S-001-2003 Method of test for fracture energy of concrete by use of notched beam*. Japan: Japanese Concrete Institute.
- JSCE. 2008. Recommendations for design and construction of high performance fibre reinforced cement composites with fine multiple cracks.
- Juhász, K.P. 2013. Modified fracture energy method for fibre reinforced concrete. In: *Fibre Concrete 2013, 12 - 13 September 2013, Prague Czech Republic*. p.8.
- Karamloo, M., Mazloom, M. and Payganeh, G. 2016. Effects of maximum aggregate size on fracture behaviours of self-compacting lightweight concrete. *Construction and Building Materials*. **123**, p8.
- Karihaloo, B.L. 1995. *Fracture Mechanics and Structural Concrete*. Essex: Longman Scientific and Technical.

- Keerthy, M.S. and Kishen, J.M. 2016. Influence of aggregate bridging on the fatigue behaviour of concrete. *International Journal of Fatigue*. **90**, p10.
- Kosmatka, S.H. and Wilson, M.L. 2016. *Design and Control of Concrete Mixtures*. 16th ed. USA: Portland Cement Association.
- Lee, J. 2017. Influence of concrete strength combined with fiber content in the residual flexural strengths of fiber reinforced concrete. *Composite Structures*. **168**, p9.
- Lydon, F.D. 1982. *Concrete Mix Design*. 2nd ed. London: Applied Science.
- Martinez, D.M. 2006. *Analysis of fibre reinforced concrete elements*. MSc (Eng) thesis, Chalmers.
- Mobley, J.A. 2009. *Birds of the world*. New York: Marshall Cavendish.
- Naanman, A.E. 2003. Engineered steel fibres with optimal properties for reinforcement of cement composites. *Journal of Advanced Concrete Technology*. **1**(3), p12.
- Owens, G. ed. 2013. *Fundamentals of concrete*. 3rd ed. Midrand, South Africa: The Concrete Institute.
- Ozbolt, J., Eligehausen, R. and Petrangeli, M. 1994. The Size Effect in Concrete Structures. In: Mihasi, H.O., H. Bazant, Z.P. ed. *Size Effect in concrete structures*. London: E&FN Spon, p.576.
- Paegle, L., Fischer, G. and Jonsson, J. 2015. *Characterization and modeling of fiber reinforced concrete for structural applications in beams and plates*. Denmark: Technical University of Denmark, Department of Civil Engineering.
- Prokorpiski, G. and Langier, B. 2000. Effect of water/cement ratio and silica fume addition on the fracture toughness and morphology of fractures surfaces of gravel concretes. *Cement and Concrete Research*. **30**, p7.
- Purnell, P. 2010. Fibre-Reinforced cements and concrete. In: Domone, P.I., J. ed. *Construction Materials*. 4th ed. Oxon: Spon Press.
- Purnell, P. 2018. Fibre Composites. In: Soutsos, M.E., Domone, P. (Ed). ed. *Construction Materials*. 5th ed. Boca Raton: CRC Press, p.820.
- Rao, G.A. 2001. Generalization of Abrams' law for cement mortars. *Cement and concrete Research*. **31**, p8.
- RILEM_TC_162-TDF. 2001. Test and design methods for steel fibre reinforced concrete . Uni-axial tension test for steel fibre reinforced concrete. Recommendations. *Materials and Structures*. **34**, p3.
- RILEM_TC_162-TDF. 2002. Test and Design Methods for Steel Fibre Reinforced Concrete. . *Materials and Structures*. **35**(November 2002), p4.
- RILEM_TC_162-TDF. 2003. Test and design methods for steel fibre reinforced concrete (Sigma Epsilon) design method Final Recommendation. *Materials and Structures*. **36**, p8.
- Shi, Z. 2009. *Crack Analyses in Structural Concrete - Theory and Applications*. Burlington: Butterworth-Heinemann.
- Simon, K.M. and Kishen, J.M.C. 2016. Influence of aggregate bridging on the fatigue behaviour of concrete. *International Journal of fatigue*. **90**, p200.
- Siriga, A.P.N., Rafiq, M.I. and Mulheron, M. 2017. Experimental investigation of the effects of aggregate size distribution on the fracture behaviour of high strength concrete. *Construction and Building Materials*. **150**, p8.
- Soutsos, M.N.L., A.P. 2012. Flexural performance of fibre reinforced concrete made with steel and synthetic fibres. *Construction and Building materials*. **36**, p7.
- The-Concrete-Society. 2007. *Guidance on the use of Macro-synthetic-fibre-reinforced-concrete*. Camberly: The Concrete Society.
- The_Concrete_Institute. 2013. *Fibre Reinforced Concrete*. [Leaflet]. Midrand: The concrete Institute.
- van Mier, J.G.M. 2013. *Concrete Fracture - A multiscale approach*. Boca Raton: Taylor & Francis.

- Weiss, J., Prof. 2011. *Stress Strain behaviour of concrete*. [Online]. [Accessed 22 July]. Available from: http://www.theconcreteportal.com/cons_rel.html
- Wittman, F.H. 1983. Structure of concrete with respect to crack formation. In: *Fracture of Non-Metallic Materials - 5th Advanced Seminar on Fracture Mechanics, Ispra, Italy*. D. Riedel Publishing Company, pp.309 - 340.
- Yin, S., Tuladhar, T., Shi, F., Combe, M., Collister, T. and Sivakugan, N. 2015. Use of macro plastic fibres in concrete: A Review. *Construction and Building Materials*. **93**, pp.180-188.
- Zollo, R.F. 1997. Fibrer-reinforced Concrete: an Overview after 30 Years of Development. *Cement and Concrete Composites*. **19**, p15.

Appendix 1. Raw measurements

The following 21 tables are the summary of the raw data measurements for each individual beam tested.

FRC L0 1					
Deflection mm	CMOD mm	CTOD mm	No 1 mm	No 2 mm	Crack length mm
1.717	0.16872205	0.105	0.014	0.025	46.1211344
2	0.31508337	0.207	0	0.019	175.255
3	0.8497092	0.606	0.285	0.058	224.36
4	1.32843421	0.984	0.579	0.06	228.85
5	1.86611254	1.529	0.784	0.309	228.85
6	2.44445044	2.186	1.172	0.317	235.52
7	3.18338805	2.717	1.547	0.614	239.02
8	3.91826955	3.341	1.975	0.746	240.01
9	4.6165703	3.912	2.221	0.927	242.7
10	5.24881257	4.467	2.547	1.167	244.46
11	6.02337621	5.062	2.851	1.285	245.61
12	7.304196	5.316	3.23	1.528	245.71
13	9.22555416	6.476	3.594	1.809	246.48
14	9.9372142	7.596	3.96	1.845	247.36
15	11.3809554	8.696	4.295	2.06	247.71
Unload	d not measure				
Span	1000				
Length	1050				
Width	301				
Height	301				
Notch	51.31				

FRC L0 2					
Deflection mm	CMOD mm	CTOD mm	No 1 mm	No 2 mm	Crack length mm
2	0.28662423	0.256	0.137	-0.04	190.02
3	0.74095444	0.636	0.402	0.069	217.38
4	1.22882676	0.998	0.668	0.199	231.86
5	1.70755306	1.469	0.965	0.329	234.01
6	2.41904008	2.062	1.394	0.537	239.82
7	3.15086241	2.64	1.792	0.725	241.16
8	4.18457794	3.442	2.304	0.943	242.37
9	4.80969781	3.832	2.708	1.165	242.94
10	5.52834454	4.417	2.708	1.356	242.95
11	6.88029885	4.962	3.024	1.557	244.98
12	8.33398218	5.53	3.414	1.747	245.04
13	9.63526371	6.67	3.792	1.926	246.93
14	10.9773054	7.75	4.163	2.073	247.42
15	12.2686156	8.85	4.53	2.301	247.59
Unload	10.2351029	7.06	3.927	1.958	
Span	1000				
Length	1050				
Width	301				
Height	300				
Notch	50.23				

FRC L0 3					
Deflection mm	CMOD mm	CTOD mm	No 1 mm	No 2 mm	Crack length mm
2	0.07419705	0.232	0.119	-0.059	161.34
3	0.67997048	0.565	0.342	0.146	203.64
4	1.11702257	0.932	0.585	0.353	222.6
5	1.61506014	1.342	0.868	0.387	225.33
6	2.27470937	1.901	1.235	0.559	233.26
7	3.11833679	2.614	1.706	0.794	234.61
8	3.85118448	3.226	2.128	1.011	238.59
9	4.55456641	3.795	2.509	1.201	240.75
10	5.23661487	4.35	2.892	1.425	242.15
11	6.47673888	4.916	3.264	1.606	243.17
12	7.97106113	5.996	3.644	1.811	243.86
13	9.39431683	7.116	4.041	2.018	244.07
14	10.553331	8.196	4.383	2.192	244.17
15	11.9056143	9.296	4.742	2.37	244.6
unload	9.87214701	7.546	4.258	2.102	
Span	1000				
Length	1050				
Width	300				
Height	300				
Notch	50.83				

Plain M 01	
Deflection mm	CMOD mm
1.41	0.35054059

FRCML0 2					
Deflection mm	CMOD mm	CTOD mm	No 1 mm	No 2 mm	Crack length mm
1.2	0.43740929	0.337	0.01	0.006	159.456667
2	0.92898479	0.749	0.145	0.026	167.636667
3	1.47064023	1.084	0.308	0.09	171.986667
4	2.10836844	1.716	0.635	0.259	173.246667
5	2.73792895	2.413	1.059	0.485	179.226667
6	3.42677863	2.871	1.507	0.731	181.048667
7	4.09213678	3.394	1.797	0.812	181.286667
8	4.7738664	3.953	2.257	1.016	182.106667
9	5.68151098	4.508	2.325	1.232	182.976667
10	6.88768806	5.118	2.708	1.375	184.086667
11	8.31887536	5.781	3.102	1.543	184.346667
12	9.35147758	6.821	3.411	1.746	185.136667
unload	6.61169028	5.134	2.685	1.365	
Span	700				
Length	750				
Width	301				
Height	223				
Notch	36.0533333				

FRC M0 3					
Deflection mm	CMOD mm	CTOD mm	No 1 mm	No 2 mm	Crack length mm
1.067	0.1665834	0.085	0.139	0.076	136.88
2	0.73480716	0.511	0.434	0.211	173.05
3	1.35208892	0.988	0.778	0.39	175.82
4	2.00821191	1.534	1.105	0.556	179.62
5	2.66229941	2.085	1.46	0.727	181.51
6	3.3225304	2.651	1.855	0.948	181.72
7	3.98686394	3.191	2.205	1.108	181.92
8	4.69618701	3.859	2.483	1.308	182.96
9	5.37078098	4.178	2.864	1.467	183.36
10	6.94493268	4.778	3.269	1.663	183.6
11	7.97742076	5.343	3.713	1.846	183.79
12	9.52120154	5.856	3.957	2.027	183.8
Unload	6.855	7.00626646	4.943	3.305	1.695
Span	700				
Length	750				
Width	300				
Height	225				
Notch	38.2				

FRC M0 4					
Deflection mm	CMOD mm	CTOD mm	No 1 mm	No 2 mm	Crack length mm
1	0.35462853	0.071	0.091	0.017	138.72
2	0.76444478	0.433	0.49	0.008	172.07
3	1.31325318	0.937	0.761	0	175.21
4	1.96528775	1.579	1.096	0	178.47
5	2.66740951	2.061	1.488	0	185.03
6	3.47992493	2.671	1.844	0	185.7
7	4.3762735	3.325	2.26	0	186.33
8	4.85461237	3.591	2.582	0	187.22
9	5.55272093	4.188	2.961	0	187.27
10	6.82022146	4.768	3.349	0	187.35
11	8.22073176	5.304	3.646	0	187.41
12	9.333	9.5396055	6.424	4.009	0
Unload	6.843	6.99399968	4.314	3.346	0
Span	700				
Length	749				
Width	301				
Height	226				
Notch	37.61				

FRC S 01			
Deflection mm	CMOD mm	CTOD mm	No 1 mm
1.5	0.31000287	0.283	0.001
2	0.60140615	0.514	0.002
3	1.17904988	0.996	0.18
4	1.7691029	1.486	0.381
5	2.38293796	1.982	0.59
6	3.0040271	2.611	0.811
7	3.20451702	3.123	1.033
8	3.62100802	3.642	1.254
9	3.82770838	4.138	1.469
10	4.44369778	4.645	1.69
unload	2.61545618	3.693	1.3
Height	150		
Span	500		
Length	550		
Width	299		
Depth	123.54		
Notch	26.46		

FRC S 02			
Deflection mm	CMOD mm	CTOD mm	No 1 mm
0	0	0	0
1	0.20967658	0.083	0.039
2	0.79360891	0.59	0.483
3	1.42912351	1.125	0.649
4	2.04191635	1.549	0.899
5	2.67332785	2.192	1.188
6	3.20038318	2.828	1.45
7	3.81427275	3.358	1.708
8	4.44473135	3.905	1.974
9	5.06282556	4.43	2.235
10	5.68923246	4.977	2.5
unload	4.58426419	4.019	2.022
Height	150		
Span	500		
Length	551		
Width	300		
Depth	125.68		
Notch	24.32		

FRC S 03			
Deflection mm	CMOD mm	CTOD mm	No 1 mm
0	0	0	0
1.1	0.44227092	0.36	0.108
2	0.9682453	0.895	0.353
3	1.58206206	1.263	0.624
4	2.1834913	1.738	0.883
5	2.90998379	2.24	1.138
6	3.5341949	2.728	1.391
7	4.14603412	3.21	1.677
8	4.739303	3.691	1.919
9.18	5.47939123	4.27	2.237
10	6.73025529	4.664	2.425
unload	5.96420529	3.665	1.913
Height	150		
Span	500		
Length	551		
Width	299		
Depth	121.01		
Notch	28.99		

Plain Concrete S04			
Deflection mm	CMOD mm	CTOD mm	No 1 mm
0.738	0.323	0.255	0.124
1	0.515	0.528	0.248
1.5	0.855	0.724	0.471

FRC ST 01		
Deflection mm	CMOD mm	CTOD mm
0.456	0.337	0.175
1	0.482	0.374
2	1.093	0.84
3	1.669	1.353
4	2.287	1.861
5	2.862	2.369
6	3.419	2.825
7	4.038	3.326
Height	150	
Span	500	
Width	150	
Depth	124.63	
Notch	25.37	

FRC ST 02		
Deflection mm	CMOD mm	CTOD mm
0.611	0.223	0.169
1	0.441	0.363
2	1.016	0.861
3	1.616	1.366
4	2.215	1.865
5	2.831	2.403
6	3.387	2.567
7	3.993	3.173
Height	150	
Span	500	
Width	150	
Depth	122.6	
Notch	27.4	

FRC ST 03		
Deflection mm	CMOD mm	CTOD mm
0.6	0.212	0.168
1	0.44	0.364
2	1.011	0.846
3	1.591	1.337
4	2.186	2.337
5	2.77	2.833
6	3.36	3.342
7	3.951	3.846
Height	150	
Span	500	
Width	150	
Depth	124.63	
Notch	25.37	

FRC ST 04		
Deflection mm	CMOD mm	CTOD mm
0.8	0.266	0.001
1	0.378	0.066
2	1	0.574
3	1.534	1.04
4	2.125	1.543
5	2.711	1.877
0.071	3.293	2.373
0.575	3.885	2.874
Height	150	
Span	500	
Width	150	
Depth	123.34	
Notch	26.66	

FRC ST 05		
Deflection mm	CMOD mm	CTOD mm
0.6	0.248	0.209
1	0.494	0.425
2	1.099	0.925
3	1.678	1.44
4	2.277	1.949
5	2.854	2.448
6	3.427	2.939
7	4.015	3.439
Height	150	
Span	500	
Width	150	
Depth	122.7	
Notch	27.3	

FRC ST 06			
Deflection mm	CMOD mm	CTOD mm	No 1 mm
0.85	0.293	0.233	0.106
1	0.372	0.289	0.152
2	0.957	0.779	0.394
3	1.536	1.295	0.66
4	2.103	1.785	0.93
5	2.7	2.225	1.183
0	3.277	2.796	1.445
0	3.876	3.235	1.665
Height	150		
Span	500		
Width	150		
Depth	122.8		
Notch	27.2		

FRC ST 07			
Deflection mm	CMOD mm	CTOD mm	No 1 mm
0	0	0	0
0.7	0.335	0.264	0.161
1	0.514	0.402	0.189
2	1.075	0.909	0.448
3	1.656	1.43	0.711
4	2.196	1.881	0.955
5	2.78	2.365	1.269
6	3.354	2.86	1.469
7	3.957	3.372	1.739
Height	150		
Span	500		
Width	150		
Depth	123.1		
Notch	26.9		

Plain Concrete ST 08		
Deflection mm	CMOD mm	CTOD mm
0	0.185	0.138
0.317	0.269	0.281
0.6	0.531	0.44
0.9	0.583	0.49
1	0.713	0.613
1.2	1.186	1.009
2	1.482	1.269
2.5		
Height	150	
Span	500	
Width	150	
Depth	123.04	
Notch	26.96	

ST09 - Plain concrete ST09		
Deflection mm	CMOD mm	CTOD mm
0.4	0.11	0.143
0.6	0.242	0.238
1	0.509	0.479
1.5	0.853	0.747
Height	150	
Span	500	
Width	150	
Depth	124.2	
Notch	25.8	

Plain Concrete ST 10		
Deflection mm	CMOD mm	CTOD mm
0.46	0.16	0.135
1	0.527	0.504
1.5	0.826	0.695
Height	150	
Span	500	
Width	150	
Depth	122.8	
Notch	27.2	

Appendix 2. Summaries of results Load/Force-CMOD

The following 2 tables are a summary of the results showing either the load (N) – CMOD in the first table and Force – CMOD in the second table. Showing the maximum force or load and the forces or loads relevant to CMOD 0.5mm, CMOD 1.5mm, CMOD 2.5mm, CMOD 3.5mm.

Summary of Load (N) - CMOD (mm) Results									
Large Beams (300 x 300 x 1000)									
	fMax	f1 (0.5)	f2 (1.5)	f3 (2.5)	f4 (3.5)	4	Span	Height	width
L01	37783	38185	46535	42383	31736	27763.37	1000	249.69	300
L02	41919	37612	51894	43281	35225	32232.98	1000	249.77	300
L03	41661	40332	59739	53452	38658	34812.58	1000	249.17	300
Mean	40455	38710	52723	46372	35206				
COV %	5.7	3.7	12.6	13.3	9.8				
Medium Beams (225 x 300 x 700)									
M01	42592.44	30774.51	36004.24	32321.6	25383.17	23357.24	700	186.95	300
M02	34119.94	24975.07	30380.26	26864.52	22538.13	19912.66	700	186.8	300
M03	36464.78	28891.82	41221.29	35078.82	27909.76	25476.31	700	188.39	300
Mean	37725.72	28213.8	35868.6	31421.65	25277.02				
COV %	11.6	10.5	15.1	13.3	10.6				
Small Beams (150 x 300 x 500)									
S01	28985.68	28907.47	24832.04	21074.83	14465.6	11525.19	500	123.54	300
S02	28056.2	15802.13	20265.87	18349.64	14451.11	12711.25	500	125.68	300
S03	28638.52	27988.32	21360.55	19988.67	16296.51	14356.34	500	121.01	300
Mean	28560.14	24232.64	22152.82	19804.38	15071.07				
COV %	1.6	30.2	10.8	6.9	7.0				
Standard Beams (150 x 150x500)									
ST1	15441.36	15439.9	10899.93	9340.12	7247.072	6534.183	500	122.12	150
ST2	14732.87	14689.39	10807.82	10045.23	7601.049	6873.44	500	122.6	150
ST3	16015.89	14596.38	12557.82	10909.28	8343.425	7671.494	500	124.63	150
ST 4	15540.46	10731.44	11696.57	11130.97	9949.512	9228.594	500	124.34	150
ST5	13954.78	8240.211	6820.36	5799.43	4702.796	4045.884	500	122.7	150
ST6	14721.58	10891.32	11331.58	9979.904	8131.641	6973.91	500	122.77	150
ST7	15113.09	11435.37	7166.14	6257.951	4953.575	4530.917	500	123.07	150
Mean	15074	12289	10183	9066	7276				
COV %	4.5	21.7	22.2	23.9	25.8				

Summary of Residual Flexural Tensile Strengths (Mpa)								
Large Beams (300 x 300 x 1000)								
	fMax	f1 (0.5)	f2 (1.5)	f3 (2.5)	f4 (3.5)	Span	Height	width
L01	3.0	3.2	3.7	3.4	2.5	1000	249.69	300
L02	3.4	3.3	4.2	3.5	2.8	1000	249.77	300
L03	3.0	3.8	4.8	4.3	3.1	1000	249.17	300
Mean	3.1	3.4	4.2	3.7	2.8			
COV %	6.2	9.3	12.8	13.5	10.0			
Medium Beams (225 x 300 x 700)								
M01	4.3	2.8	3.6	3.3	2.6	700	186.95	300
M02	3.4	2.5	3.0	2.7	2.3	700	186.8	300
M03	3.6	3.1	4.1	3.5	2.8	700	188.39	300
Mean	3.8	2.8	3.6	3.1	2.5			
COV %	12.4	10.3	14.3	12.7	9.8			
Small Beams (150 x 300 x 500)								
S01	4.7	3.2	4.1	3.5	2.4	500	123.54	300
S02	4.4	2.6	3.2	2.9	2.3	500	125.68	300
S03	4.9	2.8	3.6	3.4	2.8	500	121.01	300
Mean	4.7	2.9	3.6	3.3	2.5			
COV %	4.9	9.4	11.8	9.4	10.7			
Standard Beams (150 x 150x500)								
ST1	5.2	2.9	3.7	3.1	2.4	500	122.12	150
ST2	4.9	3.0	3.6	3.3	2.5	500	122.6	150
ST3	5.2	3.2	4.0	3.5	2.7	500	124.63	150
ST 4	5.1	2.9	3.8	3.7	3.3	500	124.34	150
ST5	4.6	1.9	2.3	1.9	1.6	500	122.7	150
ST6	4.9	2.8	3.8	3.3	2.7	500	122.77	150
ST7	5.0	1.9	2.4	2.1	1.6	500	123.07	150
Mean	5.0	2.6	3.4	3.0	2.4			
COV %	3.9	20.4	21.7	23.4	25.4			

Appendix 3. Bazant law data

These tables summarise the raw data in the first table and the calculated Bazant law data in the second table at numerous CMOD widths with the third table summarizing the Bazant law data at peak, CMOD, 0.5, 1.5, 2.5, 3.5.

	Force (N)																
CMOD	L1	L2	L3	M2	M3	M4	S1	S2	S3	ST1	ST2	ST3	ST4	ST5	ST6	ST7	
0	0	0	0	0	0	0	0	0	0	0	0	0	0	0	0	0	
0.1	37783.37	41918.96	41661.22	42592.44	34119.94	36464.78	28985.68	28056.2	28638.52	15441.36	14732.87	16015.89	15540.46	13954.78	14721.58	15113.09	
0.2	31864.82	38059.46	41922.87	22000.64	19439.82	15540.36	15151.53	14159.79	12339.01	763.5112	1795.192	932.4505	4297.816	873.0689	2268.026	1122.438	
0.4	38914.22	39648.32	45140.93	27199.98	24261.19	30961.83	18281.41	16024.27	15757.45	8194.591	8670.021	9401.755	8523.562	5544.029	7905.504	5473.036	
0.6	39858.06	42899.58	48222.81	29113.77	26075.52	33490.83	20028.36	17191.88	17033.11	8767.172	9398.343	10359.7	9264.426	5858.519	8775.434	5833.211	
0.8	41100.27	45720.7	51266.07	31584.5	27386.99	36580.19	21618.03	18179.12	18444.58	9369.145	9932.384	11186.56	9981.383	6254.893	9585.308	6295.783	
1	43068.18	48303.05	54777.41	33426.84	28663.7	38665.14	23024.08	18922.39	19516.72	9951.453	10338.83	11718.13	10624.76	6475.707	10191.73	6571.176	
1.2	44960.31	50296.44	57160.89	34889.87	29629.05	40284.04	24045.41	19574.79	20340.15	10361.41	10551.16	12139.11	11095.29	6621.645	10623.66	6835.241	
1.4	46181.64	51335.7	59018.9	35818.1	30252.31	40989.68	24599.67	20082.76	21054.04	10730.08	10733.12	12430.8	11523.05	6738.984	11126.02	7069.087	
1.6	46948.73	52140.77	60190.76	36124.8	30518.35	41452.9	24938.52	20432.51	21315.63	10988.79	10870.15	12635.54	11824.08	6876.619	11450.86	7244.711	
1.8	47323.98	51610.49	59813	36456.57	30348.99	41621.78	24761.91	20464.77	21679.95	10811.74	10997.64	12334.54	12145.33	6980.189	11616.95	7086.521	
2	46625.08	50530.9	59287.02	36397.26	29688	40622.73	24294.05	20194.39	21652.5	10647.45	11072.6	11974.49	12184.14	6724.446	11378.71	6849.557	
2.2	45694.89	47118.76	57452.7	34950.44	28458.55	38865.15	23022.9	19699.06	21067.82	10163.23	10769.14	11566.2	11944.41	6379.855	11014.05	6582.35	
2.4	43429.12	44270.39	54795.19	33099.63	27428.18	36144.04	21526.75	18918.1	20333.54	9536.933	10293	11058.44	11399.67	6042.819	10385.96	6363.86	
2.6	41308.59	42338.19	52237.51	31344.62	26454.75	34236.03	20622.9	17890.76	19612.7	9138.929	9659.4	10655.78	10876.67	5609.794	9756.132	6052.899	
2.8	39160.25	40469.53	50143.75	29777.42	25681.28	32685.77	19747.17	16920.48	18920.52	8774.445	9035.048	10033.56	10505.33	5377.382	9255.018	5553.978	
3	36899.45	38625.61	46864.67	28416.12	24785.88	31147.03	18537	16152.24	18309.02	8300.203	8568.158	9447.783	10384.58	5130.432	8904.215	5287.462	
3.2	34851.19	36964.12	43198.46	26920.25	23737.93	29805.51	16299.18	15350.11	17607.92	7833.224	8137.273	9060.299	10165.94	4958.879	8670.774	5196.492	
3.4	32665.57	35804.74	39545.98	25835.25	22892.89	28490.46	14990.93	14724.89	16814.41	7436.925	7852.405	8521.335	10050.35	4803.175	8320.637	5049.616	
3.6	30761.44	34680.4	37785.72	24904.26	22182.28	27376.81	13906.06	14054.72	15863.62	7044.419	7368.548	8212.309	9877.005	4559.816	7942.646	4838.837	
3.8	29208.61	33643.44	36266.61	24146.54	21022.16	26310.92	12115.86	13179.21	15134.55	6734.132	7014.077	7988.947	9542.926	4315.329	7462.908	4676.857	
4	27763.37	32232.98	34812.58	23357.24	19912.66	25476.31	11525.19	12711.25	14356.34	6534.183	6873.44	7671.494	9228.594	4045.884	6973.91	4530.917	

| LOP- Mpa |
|----------|----------|----------|----------|----------|----------|----------|----------|----------|----------|----------|----------|----------|----------|----------|----------|----------|----------|
| CMOD | L1 | L2 | L3 | M2 | M3 | M4 | S1 | S2 | S3 | ST1 | ST2 | ST3 | ST4 | ST5 | ST6 | ST7 | |
| 0 | 0 | 0 | 0 | 0 | 0 | 0 | 0 | 0 | 0 | 0 | 0 | 0 | 0 | 0 | 0 | 0 | |
| 0.1 | 3.03 | 3.36 | 3.36 | 4.31 | 3.42 | 3.60 | 4.75 | 4.44 | 4.89 | 5.18 | 4.90 | 5.16 | 5.11 | 4.63 | 4.88 | 4.99 | |
| 0.2 | 2.56 | 3.05 | 3.38 | 2.22 | 1.95 | 1.53 | 2.48 | 2.24 | 2.11 | 0.26 | 0.60 | 0.30 | 1.41 | 0.29 | 0.75 | 0.37 | |
| 0.4 | 3.12 | 3.18 | 3.64 | 2.75 | 2.43 | 3.05 | 2.99 | 2.54 | 2.69 | 2.75 | 2.88 | 3.03 | 2.80 | 1.84 | 2.62 | 1.81 | |
| 0.6 | 3.20 | 3.44 | 3.88 | 2.94 | 2.62 | 3.30 | 3.28 | 2.72 | 2.91 | 2.94 | 3.13 | 3.33 | 3.04 | 1.95 | 2.91 | 1.92 | |
| 0.8 | 3.30 | 3.66 | 4.13 | 3.19 | 2.75 | 3.61 | 3.54 | 2.88 | 3.15 | 3.14 | 3.30 | 3.60 | 3.28 | 2.08 | 3.18 | 2.08 | |
| 1 | 3.45 | 3.87 | 4.41 | 3.38 | 2.88 | 3.81 | 3.77 | 2.99 | 3.33 | 3.34 | 3.44 | 3.77 | 3.49 | 2.15 | 3.38 | 2.17 | |
| 1.2 | 3.61 | 4.03 | 4.60 | 3.53 | 2.97 | 3.97 | 3.94 | 3.10 | 3.47 | 3.48 | 3.51 | 3.91 | 3.65 | 2.20 | 3.52 | 2.26 | |
| 1.4 | 3.70 | 4.11 | 4.75 | 3.62 | 3.03 | 4.04 | 4.03 | 3.18 | 3.59 | 3.60 | 3.57 | 4.00 | 3.79 | 2.24 | 3.69 | 2.33 | |
| 1.6 | 3.77 | 4.18 | 4.85 | 3.65 | 3.06 | 4.09 | 4.09 | 3.23 | 3.64 | 3.69 | 3.62 | 4.07 | 3.89 | 2.28 | 3.80 | 2.39 | |
| 1.8 | 3.80 | 4.14 | 4.82 | 3.69 | 3.04 | 4.10 | 4.06 | 3.24 | 3.70 | 3.63 | 3.66 | 3.97 | 3.99 | 2.32 | 3.85 | 2.34 | |
| 2 | 3.74 | 4.05 | 4.77 | 3.68 | 2.98 | 4.01 | 3.98 | 3.20 | 3.70 | 3.57 | 3.68 | 3.85 | 4.00 | 2.23 | 3.77 | 2.26 | |
| 2.2 | 3.66 | 3.78 | 4.63 | 3.53 | 2.85 | 3.83 | 3.77 | 3.12 | 3.60 | 3.41 | 3.58 | 3.72 | 3.93 | 2.12 | 3.65 | 2.17 | |
| 2.4 | 3.48 | 3.55 | 4.41 | 3.35 | 2.75 | 3.56 | 3.53 | 2.99 | 3.47 | 3.20 | 3.42 | 3.56 | 3.75 | 2.01 | 3.44 | 2.10 | |
| 2.6 | 3.31 | 3.39 | 4.21 | 3.17 | 2.65 | 3.38 | 3.38 | 2.83 | 3.35 | 3.07 | 3.21 | 3.43 | 3.57 | 1.86 | 3.23 | 2.00 | |
| 2.8 | 3.14 | 3.24 | 4.04 | 3.01 | 2.58 | 3.22 | 3.23 | 2.68 | 3.23 | 2.94 | 3.01 | 3.23 | 3.45 | 1.79 | 3.07 | 1.83 | |
| 3 | 2.96 | 3.10 | 3.77 | 2.87 | 2.49 | 3.07 | 3.04 | 2.56 | 3.13 | 2.78 | 2.85 | 3.04 | 3.41 | 1.70 | 2.95 | 1.74 | |
| 3.2 | 2.80 | 2.96 | 3.48 | 2.72 | 2.38 | 2.94 | 2.67 | 2.43 | 3.01 | 2.63 | 2.71 | 2.92 | 3.34 | 1.65 | 2.87 | 1.71 | |
| 3.4 | 2.62 | 2.87 | 3.18 | 2.61 | 2.30 | 2.81 | 2.46 | 2.33 | 2.87 | 2.49 | 2.61 | 2.74 | 3.30 | 1.60 | 2.76 | 1.67 | |
| 3.6 | 2.47 | 2.78 | 3.04 | 2.62 | 2.22 | 2.70 | 2.28 | 2.22 | 2.71 | 2.36 | 2.45 | 2.64 | 3.25 | 1.51 | 2.63 | 1.60 | |
| 3.8 | 2.34 | 2.70 | 2.92 | 2.44 | 2.11 | 2.59 | 1.98 | 2.09 | 2.58 | 2.26 | 2.33 | 2.57 | 3.14 | 1.43 | 2.47 | 1.54 | |
| 4 | 2.23 | 2.58 | 2.80 | 2.36 | 2.00 | 2.51 | 1.89 | 2.01 | 2.45 | 2.19 | 2.29 | 2.47 | 3.03 | 1.34 | 2.31 | 1.49 | |

Size Effect - Bazant Law					
Large Beams					
	fMax	f1 (0.5)	f2 (1.5)	f3 (2.5)	f4 (3.5)
L01	0.50	0.51	0.62	0.57	0.42
L02	0.56	0.50	0.69	0.58	0.47
L03	0.56	0.54	0.80	0.72	0.52
Mean	0.54	0.52	0.70	0.62	0.47
COV %	5.77	3.84	12.71	13.39	9.94
Medium Beams					
M02	0.76	0.55	0.64	0.58	0.45
M03	0.61	0.45	0.54	0.48	0.40
M04	0.65	0.51	0.73	0.62	0.49
Mean	0.67	0.50	0.64	0.56	0.45
COV%	11.71	10.39	14.69	12.93	10.21
Small Beams					
S01	0.78	0.78	0.67	0.57	0.39
S02	0.74	0.42	0.54	0.49	0.38
S03	0.79	0.77	0.59	0.55	0.45
Mean	0.77	0.66	0.60	0.54	0.41
COV%	3.13	31.34	11.17	8.05	8.84
Standard Beams					
ST1	0.84	0.84	0.60	0.51	0.40
ST2	0.80	0.80	0.59	0.55	0.41
ST3	0.86	0.78	0.67	0.58	0.45
ST4	0.83	0.58	0.63	0.60	0.53
ST5	0.76	0.45	0.37	0.32	0.26
ST6	0.80	0.59	0.62	0.54	0.44
ST7	0.82	0.62	0.39	0.34	0.27
Mean	0.82	0.67	0.55	0.49	0.39
COV%	4.04	21.76	21.84	23.52	25.37

Appendix 4. Equivalent angles and Bazant law data

The following tables reflect the data which has been equalized to represent the forces at an equivalent CMOD. In this case while it is all reflected as CMOD 1,2, 3....15 the large beam data at 1mm is really the 2mm data and the medium beam data is really 1.4mm CMOD. As explained in the main body. The tables show all the data in table 1 then a summary of the Load data in the second table and the third table shows the Force calculated using the Bazant size effect equation.

Load based on equivalent deflection. - CMOD2mm = on Large Beam = CMOD 1.4mm on Medium beam = 1mm on Small and standard beams																
CMOD	L1	L2	L3	M2	M3	M4	S1	S2	S3	ST1	ST2	ST3	ST4	ST5	ST6	ST7
0	0	0	0	0	0	0	0	0	0	0	0	0	0	0	0	0
Peak	37783	41919	41661	42592	34120	36465	28986	28056	28639	15441	14733	16016	15540	13955	14722	15113
1	43068	48303	54777	30389	26853	35288	28907	15802	27988	15440	14689	14596	10731	8240	10891	11435
2	46625	50531	59287	35818	30252	40990	23024	18922	19517	9951	10339	11718	10625	6476	10192	6571
3	36899	38626	46865	35819	29045	39744	24832	20266	21361	10900	10808	12558	11697	6820	11332	7166
4	27763	32233	34813	29777	25681	32686	24294	20194	21653	10647	11073	11974	12184	6724	11379	6850
5	21725	24185	27521	25383	22538	27910	21075	18350	19989	9340	10045	10909	11131	5799	9980	6258
6	18183	20433	23971	22599	19214	24394	18537	16152	18309	8300	8568	9448	10385	5130	8904	5287
7	15900	18344	21348	20525	16562	21122	14466	14451	16297	7247	7601	8343	9950	4703	8132	4954
8	14361	16516	19285	18909	14530	18008	11525	12711	14356	6534	6873	7671	9229	4046	6974	4531
9	13317	14785	16944	17378	13844	16304		11139	13204	6804	6703	7980	10321	4287	7828	4789
10	10911	13531	15052	16180	13087	14765		10140	12086	7561	7448	8867	11467	4763	8698	5321
11		12400	13421	15378	12063	13618		8961	10895	8317	8193	9754	12614	5240	9567	5853
12		11077	12477	14707	11129	12531		1229	10674	9073	8938	10640	13761	5716	10437	6385
13			11186	13573	10363	11493		12262	11057	6713	7032	8165	9925	4284	8358	4703
14			9894	24061	7457	6422				10585	10428	12414	16054	6669	12177	7449
15			8602	22738	6025	4276				11341	11172	13300	17201	7145	13047	7981
	L1	L2	L3	M2	M3	M4	S1	S2	S3	ST1	ST2	ST3	ST4	ST5	ST6	ST7
Span	1000	1000	1000	700	700	700	500	500	500	500	500	500	500	500	500	500
width	300	300	300	300	300	300	300	300	300	150	150	150	150	150	150	150
ht	249.69	249.77	249.17	186.04	186.8	188.39	123.54	125.68	121.01	122.1	122.6	124.63	123.34	122.7	122.8	123.1

Summary Load in Newtons / Equivalent Angles of Deformation Lagre beam @ 2mm = small beam @ 1mm CMOD										
Large Beams (300 x 300 x 1000)										
		fMax	f1 (0.5)	f2 (1.5)	f3 (2.5)	f4 (3.5)	4	Span	Height	width
L01	0	37783.4	43068.2	36899.5	21724.5	15899.8	14360.8	1000	249.69	300
L02	0	41919.0	48303.0	38625.6	24185.1	18344.0	16515.5	1000	249.77	300
L03	0	41661.2	54777.4	46864.7	27521.4	21348.1	19285.3	1000	249.17	300
Mean	0	40454.5	48716.2	40796.6	24477.0	18530.7	16720.6		249.5433	
COV %		5.7	12.0	13.1	11.9	14.7	14.8			
Medium Beams (225 x 300 x 700)										
M01	0	42592.4	30388.8	35818.6	25383.2	20524.9	18908.6	700	186.95	300
M02	0	34119.9	26852.7	29045.1	22538.1	16561.6	14529.5	700	186.8	300
M03	0	36464.8	35288.5	39743.9	27909.8	21122.1	18007.7	700	188.39	300
Mean	0	37725.7	30843.3	34869.2	25277.0	19402.9	17148.6		187.38	
COV %		11.6	13.7	15.5	10.6	12.8	13.5			
Small Beams (150 x 300 x 500)										
S01	0	28985.7	28907.5	24832.0	21074.8	14465.6	11525.2	500	123.54	300
S02	0	28056.2	15802.1	20265.9	18349.6	14451.1	12711.3	500	125.68	300
S03	0	28638.5	27988.3	21360.6	19988.7	16296.5	14356.3	500	121.01	300
Mean	0	28560.1	24232.6	22152.8	19804.4	15071.1	12864.3		123.41	
COV %		1.6	30.2	10.8	6.9	7.0	11.1			
Standard Beams (150 x 150x500)										
ST1	0	15441.4	15439.9	10899.9	9340.1	7247.1	6534.2	500	122.12	150
ST2	0	14732.9	14689.4	10807.8	10045.2	7601.0	6873.4	500	122.6	150
ST3	0	16015.9	14596.4	12557.8	10909.3	8343.4	7671.5	500	124.63	150
ST 4	0	15540.5	10731.4	11696.6	11131.0	9949.5	9228.6	500	124.34	150
ST5	0	13954.8	8240.2	6820.4	5799.4	4702.8	4045.9	500	122.7	150
ST6	0	14721.6	10891.3	11331.6	9979.9	8131.6	6973.9	500	122.77	150
ST7	0	15113.1	11435.4	7166.1	6258.0	4953.6	4530.9	500	123.07	150
Mean	0	15074.3	12289.1	10182.9	9066.1	7275.6	6551.2		123.1757	
COV %		4.5	21.7	22.2	23.9	25.8	27.2			

Summary Force Bazant Law / Equivalent angles of deformation Lagre beam @ 2mm = small beam @ 1mm CMOD										
Large Beams (300 x 300 x 1000)										
		fMax	f1 (0.5)	f2 (1.5)	f3 (2.5)	f4 (3.5)	4	Span	Height	width
L01	0	0.5044	0.5750	0.4926	0.2900	0.2123	0.1917	1000	249.69	300
L02	0	0.5594	0.6446	0.5155	0.3228	0.2448	0.2204	1000	249.77	300
L03	0	0.5573	0.7328	0.6269	0.3682	0.2856	0.2580	1000	249.17	300
Mean	0	0.5404	0.6508	0.5450	0.3270	0.2476	0.2234		249.54	
COV %		5.8	12.2	13.2	12.0	14.8	14.9			
Medium Beams (225 x 300 x 700)										
M01	0	0.7594	0.5418	0.6386	0.4526	0.3660	0.3371	700	186.95	300
M02	0	0.6088	0.4792	0.5183	0.4022	0.2955	0.2593	700	186.8	300
M03	0	0.6452	0.6244	0.7032	0.4938	0.3737	0.3186	700	188.39	300
Mean	0	0.6712	0.5485	0.6201	0.4495	0.3451	0.3050		187.38	
COV %		11.7	13.3	15.1	10.2	12.5	13.3			
Small Beams (150 x 300 x 500)										
S01	0	0.7821	0.7800	0.6700	0.5686	0.3903	0.3110	500	123.54	300
S02	0	0.7441	0.4191	0.5375	0.4867	0.3833	0.3371	500	125.68	300
S03	0	0.7889	0.7710	0.5884	0.5506	0.4489	0.3955	500	121.01	300
Mean	0	0.7717	0.6567	0.5986	0.5353	0.4075	0.3479		123.41	
COV %		3.1	31.3	11.2	8.0	8.8	12.4			
Standard Beams (150 x 150x500)										
ST1	0	0.8430	0.8429	0.5950	0.5099	0.3956	0.3567	500	122.12	150
ST2	0	0.8011	0.7988	0.5877	0.5462	0.4133	0.3738	500	122.6	150
ST3	0	0.8567	0.7808	0.6717	0.5836	0.4463	0.4104	500	124.63	150
ST 4	0	0.8332	0.5754	0.6271	0.5968	0.5335	0.4948	500	124.34	150
ST5	0	0.7582	0.4477	0.3706	0.3151	0.2555	0.2198	500	122.7	150
ST6	0	0.7994	0.5914	0.6153	0.5419	0.4416	0.3787	500	122.77	150
ST7	0	0.8187	0.6195	0.3882	0.3390	0.2683	0.2454	500	123.07	150
Mean	0	0.8158	0.6652	0.5508	0.4904	0.3934	0.3542		123.1757	
COV %		4.0	21.8	21.8	23.5	25.4	26.7			

Appendix 5. Previous Assignments

1. Initial research proposal Pg. 89 - 94

a. Submitted 14 December 2017

b. Equivalent words 989

2. Aims and Objectives Pg. 95 - 108

a. Submitted 19 March 2018

b. Equivalent words 3098

Not Included in this version.

